The quench prevention of the LHC Main Dipoles

–

Geant4 simulations of Beam Loss Monitors thresholds

Pre-diploma project

By Agnieszka Priebe

Poznan University of Technology
Faculty of Technical Physics

Supervisors:

Dr Mariusz Sapiński & Dr Bernd Dehning

CERN
Accelerator and Beams Department
Beam Instrumentation Group
Beam Loss Monitoring Section

Poznań 2009

Prewencja zniszczeń Głównych Dipoli LHC

–

Symulacje wartości progowych Monitorów Strat Wiązki za pomocą Geant4

Praca przejściowa

Agnieszka Priebe

Politechnika Poznańska
Wydział Fizyki Technicznej

Opiekunowie:

Dr Mariusz Sapiński & Dr Bernd Dehning

CERN
Departament Akceleratorów i Wiązek
Grupa Instrumentacji Wiązki
Sekcja Monitoringu Strat Wiązki

Poznań 2009

Acknowledgement

I would like to thank my supervisor, dr Mariusz Sapiński, especially for patience ;-) support in any cases and answering to hundreds of my questions.

I'm also grateful to dr Bernd Dehning for giving me a chance to work at CERN and participate in so great experiment as LHC is.

Last, I would like to thank all people from BL section for kindness and friendly atmosphere.

During this one year of Technical Student Program I have benefited a lot, not only from educational point of view, but I have also collected new unpredictable experiences. Thanks!

Contents

Introduction

This thesis contains results of Geant4 simulations which have been entirely done during the Technical Student Program at CERN (Geneva, Switzerland) in 2007-2008. The co-author and main coordinator of presented effects is dr Mariusz Sapiński.

The main aim of this project has been to estimate the correlation between the energy deposition inside the superconducting coils and signal. The simulations have been performed with the Geant4 Monte Carlo Code and compared with two first beam-induced quenches of the Main Dipoles.

This thesis has been divided into eight chapters:

- → Chapter 1. CERN presents general overview of the organization, highlights the history and the mission. The main facilities also have been briefly discussed.
- → Chapter 2. Theoretical basis is devoted to fundamental theoretical aspects. Such terms as the hadronic shower, the superconductivity, the superfluidity, the quench, the cross-talk have been introduced.
- → Chapter 3. The Large Hadron Collider contains the description and technical parameters of the Large Hadron Collider. It has been focused mostly on these fields, which are crucial for the preparation of the simulations. Thus the design of the Main Dipoles and the Beam Loss Monitors have been discussed here. The parameters of the proton beam have been also shown.
- → Chapter 4. Geant4 simulations is the heart of our work. It presents the entire procedure of our simulation preparation - from the design of the Geant4 geometry to the application of an appropriate model of physics .
- → Chapter 5. Data analysis – the coils consists our studies of various scenarios in regard to the loss locations and the beam energies.
- → Chapter 6. Data analysis – the Beam Loss Monitors presents final correlation between the situation inside the superconducting coils and the signal of the detectors. The results of estimated thresholds are given.
- → Chapter 7. Accuracy of the simulations shows the sources of errors which have taken place during the preparation of simulations. The margin of errors is calculated.
- → Chapter 8. Conclusions sums up the entire project, gives final remark and plans for the future.

1. CERN

CERN - the European Organization for Nuclear Research (franc. Conseil Européen pour la Recherche Nucléaire) is located astride Franco-Swiss border, between Lac Leman and Jura Mountains. It was officially founded in 1954 as one of European's first joint venture and nowadays has twenty Member States. The CERN mission is to investigate the fundamental sciences - especially High Energy Physics and Particle Physics. Precise experiments at CERN require instruments which advance to the technology frontiers.

Fig.1.1 shows the CERN facilities. The LINAC2 and the LINAC3 are linear accelerators of, correspondingly, protons and lead ions. The following accelerators: the BOOSTER, the PS (**P**roton **S**ynchrotron), the LEIR (**L**ow **E**nergy **I**on **R**ing), the SPS (Super Proton Synchrotron) and the LHC (Large Hadron Collider) are used to increase the beam energy. ALICE (**A** **L**arge **I**on **C**ollider **E**xperiment), ATLAS (**A** **T**oroidal **L**HC **A**pparatu**S**), CMS (the **C**ompact **M**uon **S**olenoid) and LHCb (**L**arge **H**adron **C**ollider **b**eauty) are interaction points where LHC beams will collide. The **A**ntiproton **D**ecelerator (AD) provides low-energy particles for studies of antimatter. The n-TOF's (the **n**eutron **t**ime-**o**f-**f**light facility) task is to examine the processes of neutrons which are related to stellar evolution. Neutrinos are objects of CNGS (The **C**ERN **N**eutrinos to **G**ran **S**asso) interests. ISOLDE (On-Line Isotope Mass Separator) group works on radioactive isotopes.

The entire World turned its attention on the first LHC start up in September 2008 and now waits for new highlights.

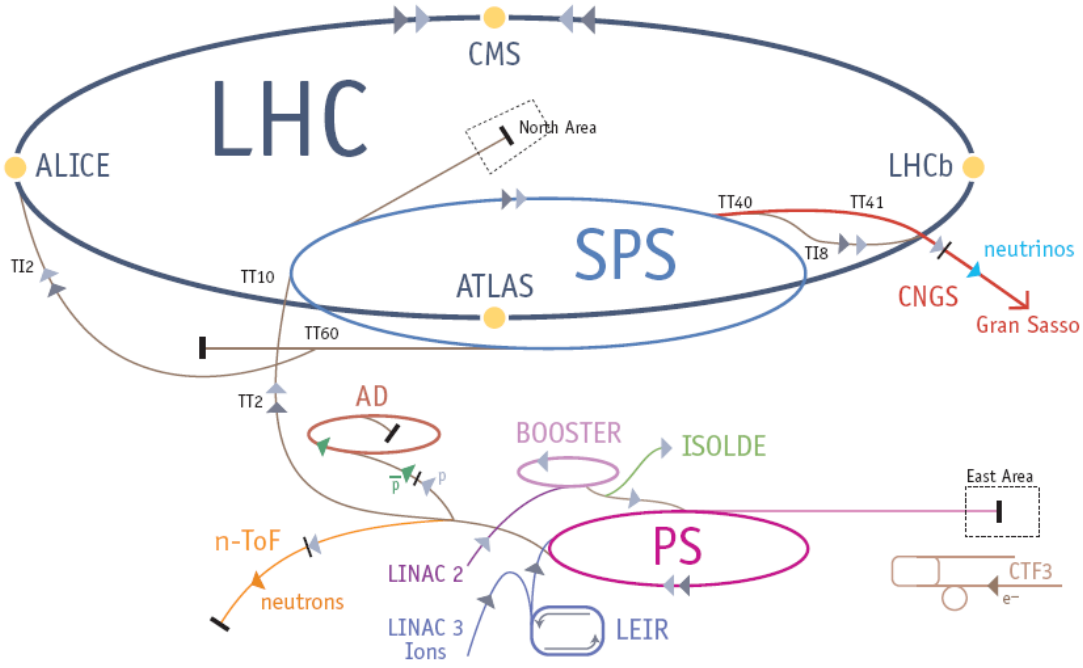

Fig.1.1: The CERN facilities, courtesy [13].

2. Theoretical basis

2.1 Hadronic Shower

Decays of unstable particles, strong inelastic and elastic nuclear interactions as well as electromagnetic interactions affect the passage of high-energy particles through a dense matter. A cascade of secondary particles is called the particles shower. Multi-particle production is the main feature of interactions when the energy is greater than a few GeV. The shower core is formed by a primary beam axis with concentrated energetic particles. At energy smaller than 100 MeV neutral particles (mainly neutrons) and photons dominate with a cascade development. The higher primary energy is, the larger shower dimensions are.

2.2 Superconductivity

Superconductivity is a phenomenon observed in a large variety of material at very low temperatures close to 0 K. The most characteristic property of superconductors is $R = 0\ \Omega$ (the electrical resistance is equal zero).

There are three conditions which must be satisfied to obtain the superconductivity state:

- Temperature $T < T_C$
- Current $I < I_C$
- Magnetic field $B\ (T) < B_C\ (T)$

where index "C" refers to the critical values. Even if one of these parameters exceeds the threshold value, the material transits to normal conducting state (Fig.2.2.1).

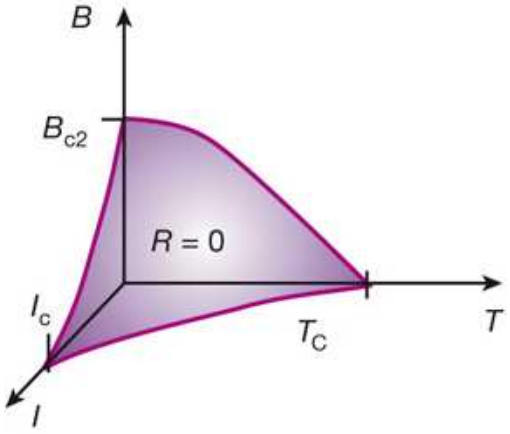

Fig.2.2.1: Magnetic-field–temperature–current (B–T–I) superconductor phase diagram [19].

We can distinguish two types of superconductors with rather different responses to magnetic field:

1) Type I superconductors (lead, tin, aluminium, mercury etc). These materials do not admit a magnetic field to the bulk. Their phase transition is of first order, which means that the applied field is below $B_C\,(T)$. Any significant applications of type I superconductors have not been found .
2) Type II superconductors (niobium-titanium, niobium-tin, niobium, lead-indium and other superconducting alloys). In comparison with type I superconductors, these ones are characterised by not one but by two critical field values: B_{c1} and B_{c2}. The Meisner phase occurs below B_{c1} (a complete field expulsion), while in the range of magnetic field $B_{c1} < B < B_{c2}$ the mixed phase is observed – magnetic field can penetrate the bulk in the form of flux tubes.

A comparison between Type I and type II superconductors is presented on Fig.2.2.2. The relation between magnetic field ***B*** and auxiliary magnetic field ***H*** is given by

$$\vec{B} = \mu_0(\vec{H} + \vec{M}), \tag{2.1}$$

where ***M*** is the magnetization and μ_0 is the vacuum permeability.

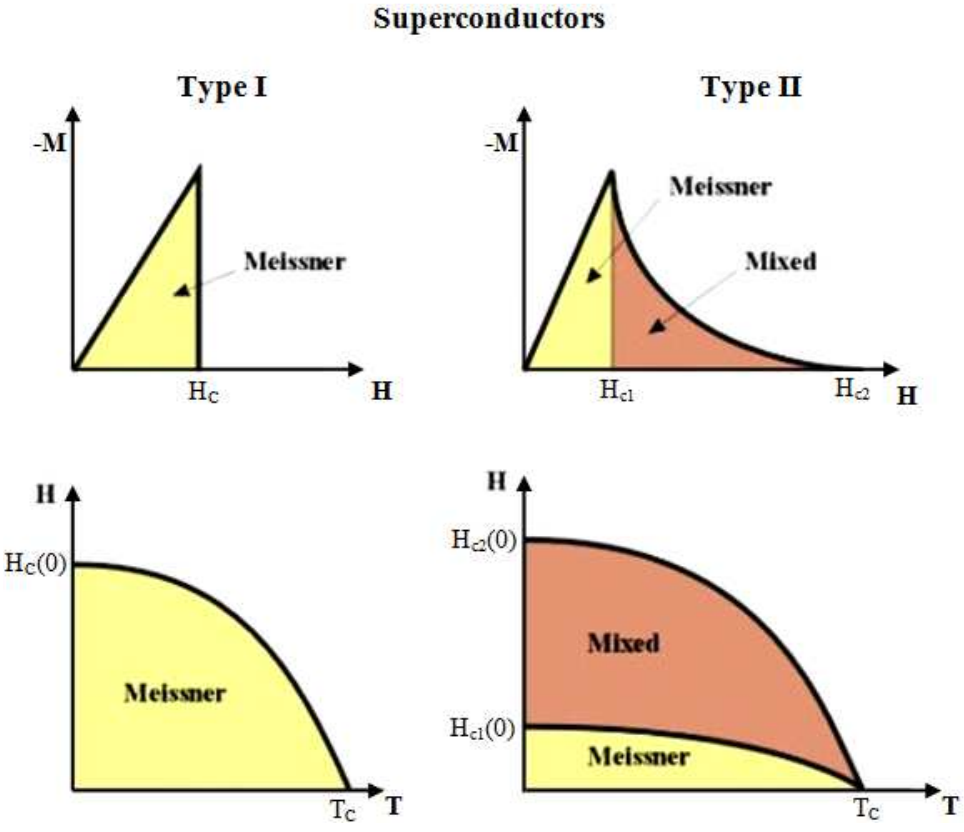

Fig.2.2.2: Magnetization properties of Type I and Type II superconductors [15].

The explanation of superconductivity is based on BCS theory which says that so-called supercurrent is not carried by single electrons but by Cooper pairs – the pairs of electrons with opposite spins and momenta. The critical temperature is related to an energy gap between BCS ground state (which is occupied by all pairs) and the single-electron state.

From mathematical point of view, superconductivity is described by London's equations.

2.3 Superfluidity

Under certain circumstances, a fluid which is composed of neutral particles can flow without friction. This effect is called a superfluidity. Currently, only few superfluids are known – two of them are isotopes of helium. ^{4}He becomes superfluid at the temperature below 2.17 K and ^{3}He below about 2 mK. A reason of the superfluidity existence is the Bose condensation.

Atoms forming the liquid ^{4}He are bosons and if the temperature is lower than critical one, a finite fraction of particles starts to occupy the lowest quantum state. They obey the Bose statistics.

As the liquid ^{3}He atoms are fermions, the Bose Condensation is concerned with Cooper pairs (like in superconductors).

The superconducting cables which form the coils of LHC magnets are immersed in a bath of superfuid helium at temperature of 1.9 K.

2.4 Physics of dipoles

Accelerator magnets requires stringent field uniformity condition in order to minimize an un-controllable beam orbit distortion and beam losses.

Dipole magnets are used to guide charge particle beams along desired orbit.
The Lorentz force law is given by:

$$\vec{F} = q\left(\vec{v} \times \vec{B}\right), \tag{2.2}$$

where q is the electric charge of particle (C), $\boldsymbol{v}$ is the velocity (m/s) and $\boldsymbol{B}$ is the magnetic field (T). Therefore the bending angle Θ is

$$\theta = \frac{e}{p_0}\int_{s_1}^{s_2} Bdl = \frac{1}{B\rho}\int_{s_1}^{s_2} Bdl, \tag{2.3}$$

where p_0 is the momentum of the beam, and $B\rho = \frac{p_0}{e}$ is the momentum rigidity of the beam. For a circular accelerator, the total bending angle is 2π, and thus the total integrated dipole field becomes

$$\oint Bdl = 2\pi \frac{p_0}{e} = 2\pi B\rho, \tag{2.4}$$

This means, the greater magnetic field is applied, the smaller the bending radius of a dipole magnet is required to obtain the desired momentum of the beam.

2.5 Quench

A quench is a termination of an exit from superconducting (non-resistive) state into a normal (resistive) state of superconducting materials.

Superconducting cables, which form the coils, are constructed of strands (see Chapter 3.3). Each strand consists of a copper matrix which surrounds the niobium-titanium (type II superconductor filaments). This structure is completely immersed in the liquid helium at the bath temperature.

The superconductor carries the current and below critical temperature the Joule heating is equal zero. When temperature is greater than critical one, practically the superconductor is free of current. While the niobium-titanium resistance exceeds the resistance of the copper by a factor 2000, a heating of the material can cause magnet damages. Therefore is undesirable effect and must be excluded.

Quenches can be induced when:

- the external magnetic field, the temperature or the current density exceeds the critical value
- even a small wire movement appears
- an epoxy is cracked
- an eddy current heating occurs
- a powering fails
- the other sources are distributed (for instance a heating by the beam)

If the quench appears, peculiar actions are brought to avoid magnet destructions. The first one is a trigger of special quench heaters, which warm the whole magnet – this causes steady resistance along the material and prevent a local giant resistance concentration. The second one is based on leading the beam to a dump – the only region in the LHC tunnel where entire energy can be deposited.

3. The Large Hadron Collider

3.1 General layout

The Large Hadron Collider (LHC) is the largest particle accelerator and collider ever built. It has been installed in the Large Electron-Positron Collider (LEP) tunnel of about 27 km. The main aims for the LHC are to discover the Higgs Boson (the God Particle) and study rare events appearing at high energies – up to 14 TeV (at centre of mass collisions). Fig. 3.1.1 presents a picture which has been made inside the LHC tunnel.

The LHC is a two-in-one ring what means that both channels with circulating beams are combine in the same mechanical structure. That was applied due to the lack of space in the LEP tunnel to separate two rings of magnets. Distance between a clockwise and a counter-clockwise beams is about 194 mm in the arc and reaches the value of about 420 mm when beams are accelerated in RF cavities.

As the beam peak energy strongly depends on integrated dipole field along the storage ring circumstance the superconducting magnet technology was used. To obtain a peak beam energy of up to 7 TeV in the LEP tunnel, the dipole field of 8.33 T had to be provided.

Fig.3.1.1: The LHC tunnel. Main Dipoles are blue, Main Quadrupoles – grey.

The LHC is made of eight arcs and eight so-called “insertions”. Each arc contains 154 bending magnets. Long straight section (LSS) plus two dispersion suppressors (DS) – one at each end - form an insertion. An octant begins in the middle of an arc and ends in the middle of the following arc. Therefore it spans a full insertion (Fig. 3.1.3). Such a nomenclature is useful from practical point of view while looking at the application of the magnets to guide the beams through injection, cleaning and dumping sections or into collision.

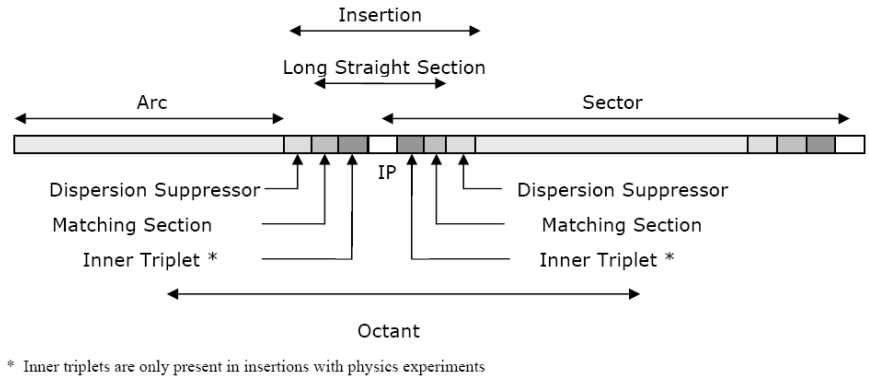

Fig.3.1.2: Octants and sectors in the LHC [1].

The magnets are powered in eight symmetric and independent sectors – parts of the machine between insertion points (Fig.3.1.3). These sectors are the LHC working units – magnet installation and commissioning happen sector by sector. Over forty different cryostats house superconducting magnets within the sectors, while normal conducting magnets are contained in LSS.

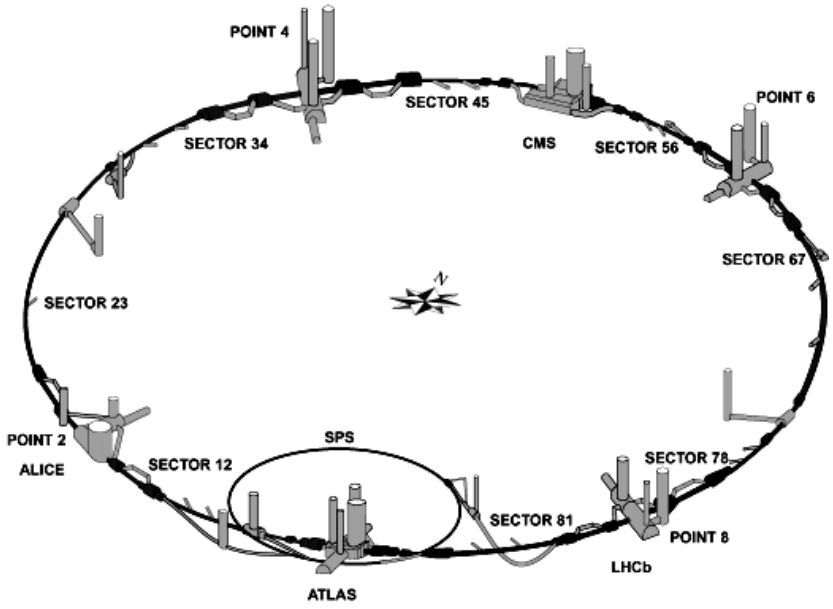

Fig. 3.1.3: The LHCs layout: sectors and interaction points [16].

3.2 The LHC beam

The LHC beam consists of either protons or lead ions. In this study only proton beams have been considered.

Hydrogen gas is a source of protons. High electric current of cathode causes that the gas becomes a plasma. An electric field separates positive charged particles from negative ones – it strips atoms from electrons. Afterwards protons are injected to a chain of accelerators: the LINAC2, the Booster, the PS and the SPS and the LHC. Fig 3.2.1 shows steps of an energy gain in the particular accelerators.

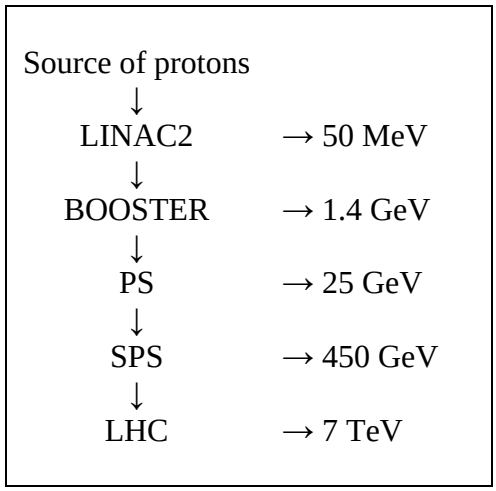

Fig. 3.2.1: Diagram of the LHC proton beam the energy gain.

Under nominal working conditions the proton beam will reach an unprecedented energy of 7 TeV.

Table 3.2.1: Some of the LHC beam parameters (based on [1] and [13]).

Proton beam	Unit	Injection 450 GeV	Collision 7 TeV
Bunch area (2σ)	eVs	1.0	2.5
Bunch length (4σ)	ns	1.71	1.06
Intensity per bunch	10^{11}	1.15	1.15
Number of bunches per beam		2808	2808
Min. distance between bunches	m		7
Design luminosity	$cm^{-2}s^{-1}$	-	10^{34}
Number of turns	s^{-1}	11 245	11 245
Number of collision	s^{-1}		600 million

The choice of protons to circulate in the LHC was due to a synchrotron radiation which is about 10^{13} smaller than in case of electrons. It is worth to underline the fact that the LHC beam is not continuous but formed into bunches (as a result of RF cavities performance). Some of main parameters of the LHC beam is shown in Tab.3.2.1.

3.3 Main Dipoles

Among all LHC magnets, the most numerous are the Main Dipoles (MB). 1104 in the arc and 128 in the dispersion suppressor region gives in total 1232 Main Dipoles accommodated in the LHC ring. Basically, they are designed in the same way. Only interconnections and some geometric details vary DS dipoles from SSS dipoles due to demands of the Dispersion Suppressor regions.

So-called "dipole cold mass" is a core of a cryodipole. Inside a shrinking cylinder/He-vessel, all components are cooled down by the liquid helium with temperature of 1.9 K. Cold mass provides two apertures for tubes where particle beam will circulates (cold bores). Parameters and a picture of Main Dipole is given on Fig.3.3.1.

Fig.3.3.2 shows a part of CDD drawing no. LHCMB_T_0035 – the cross-section of MB cold mass. Austenitic steel collars are pressed around superconducting coils, hold them in proper positions and therefore provide the structural stability of the cold mass. Any

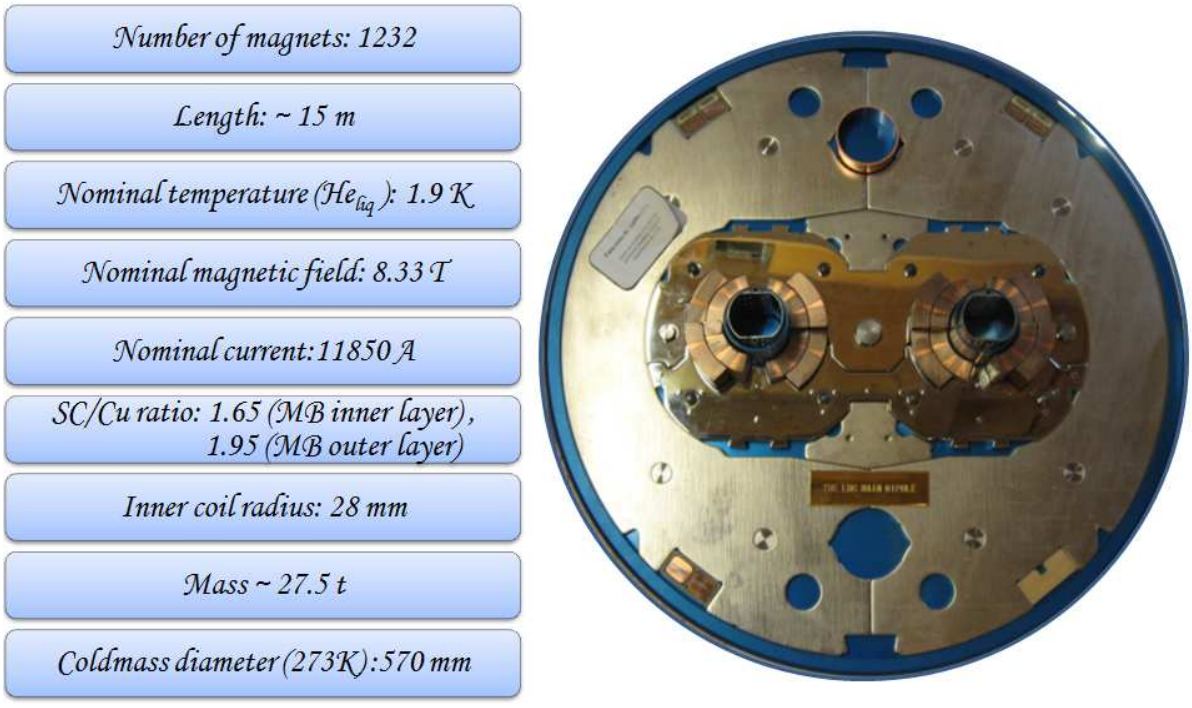

Fig. 3.3.1: The Main Dipole. On the left: the most significant parameters of MB. On the right: cross-section of Cold Mass.

deformations and displacements must be limited to avoid sudden release of energy, which can cause quenching. Between coils and surroundings (collars, iron yoke, He-vessel) a pre-stress has been built-in. Two apertures contain cold bores and beam screens. A role of the

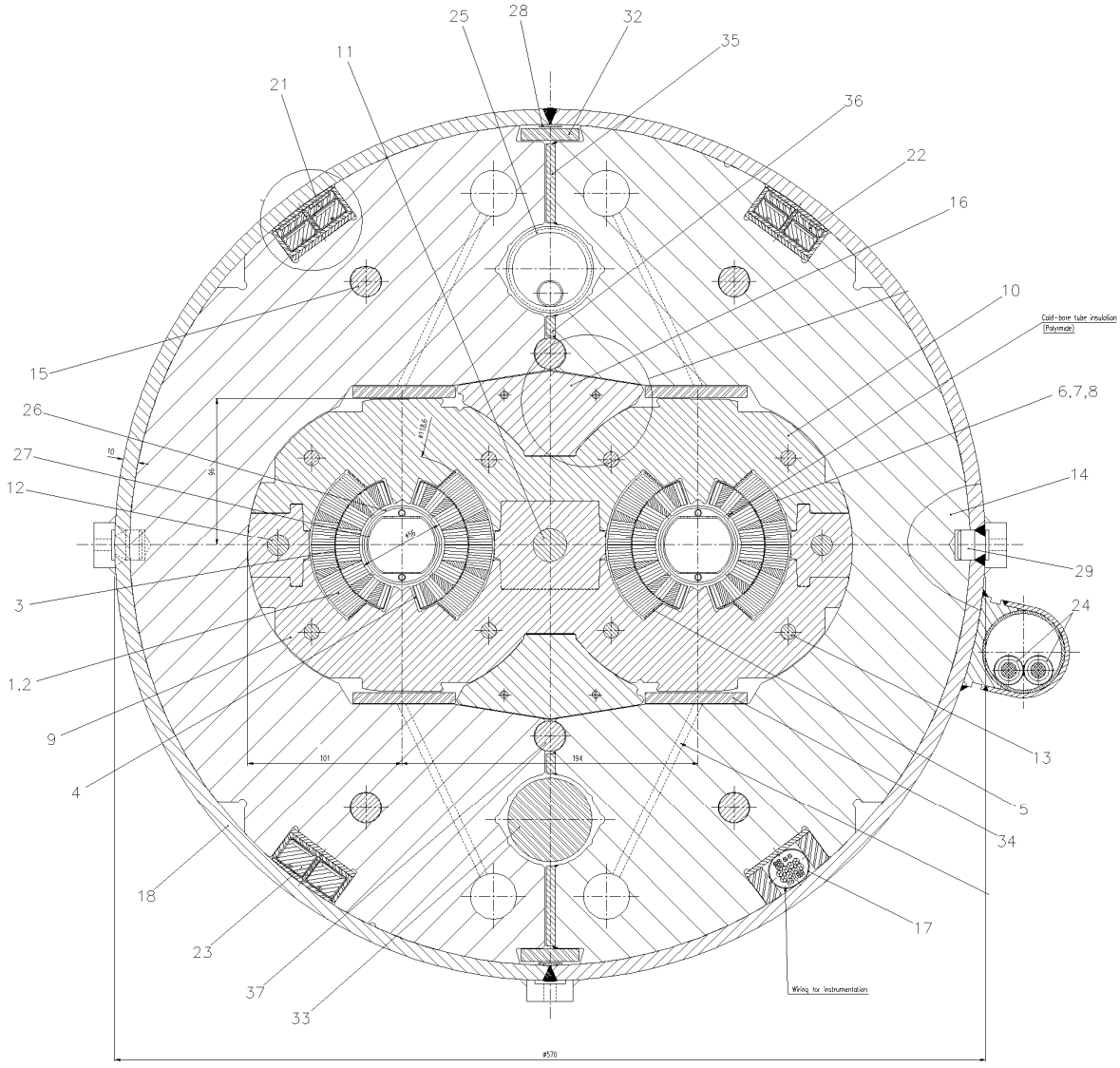

Fig.3.3.2: Drawing LHCMB_T_0035[2]; 1 - Conductor distribution, 2 – Coil assembly, 3 – Interlayer, 4 – Shim, inner layer, 5 – Shim, outer layer, 6 – Ground insulation, 7 – Quench heater type 1 and 2, 8 – Coil protection sheet, 9 – Collar A, type 1, 10 – Collar A, type 2, 11 – Control locking rod, 12 – Lateral locking rod, 13 – Collar pack assy. rod, 14 – Lamination, type A, 15 – Half core assy. rod, 16 – Insert, 17 – Glass-cloth tubing, 18 – Half – cylinder, 19 – Iron insert slide – sheet, 20 – Iron insert shim, 21 – Quadrupole "D" bus-bars, 22 - Quadrupole "F" bus-bars, 23 – Dipole bus-bars, 24 – Auxiliary bus-bars, 25 – Heat exchanger tube, 26 – Cold-bore tube, 27 – Beam screen, 28 – Backing strip, 29 – Positioning dowel pin, 30 – Antitorsion bar, 31 – Spacers, 32,33,34 – Filler pieces, 35,36 – Sheets, 37 – Round bar.

beam screen is to absorb the heat produced by the beam through an induction. The entire structure of cold mass is very complex. Every component has been designed very precisely and a wide range of miscellaneous implications of their placement has been taken into account. Each part plays its own role and none is meaningless – for instant, holes in the collars supply the required shape of magnetic field lines.

A factor, which distinguishes the LHC magnets from the others, is an application of superconducting coils. The main reason of use them is to attain a higher magnetic field than in conventional magnets. They are built of Rutherford cables (see Fig.3.3.3).

There are two kinds of cables used during a production of Main Dipole superconducting coils. The inner layers are wound from a cables consisting up to 28 twisted 15-mm strands. Each strand has been made up in turn of approximately 8900 individual filaments. The outer layers consist of 36-strand cables and a number of filaments forming the strand decreases to 6500. The main parameters of two cables are given in Tab.3.3.1

Cables are insulated with two polyimide layers wrapped around the cable with a 50% overlap, together with another polyimide tape wrapped with spacing of 2 mm. The gap is penetrated by the liquid helium. The outer layer is treated with an adhesive layer - external surface coated with epoxy resin (Fig.3.3.4).

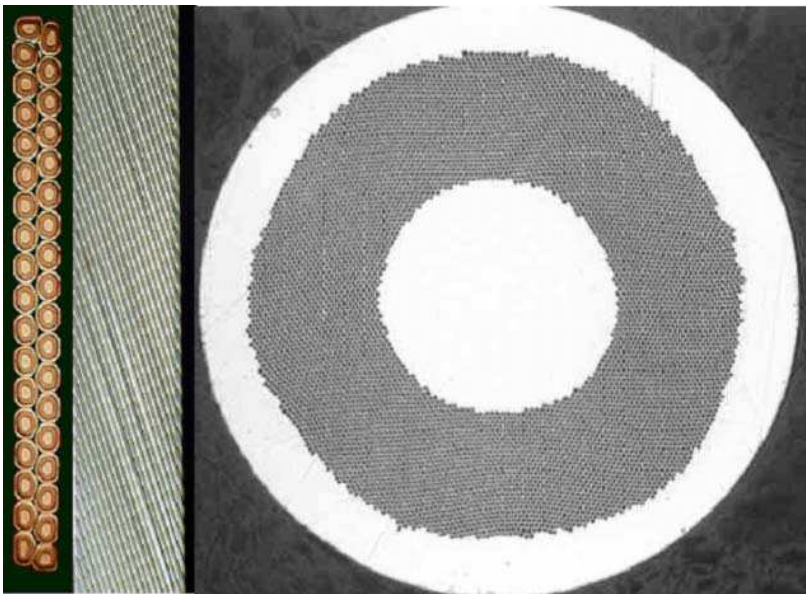

Fig.3.3.3: Structure of the Rutherford cable [1].

Table 3.3.1: Strand and cable characteristics of main dipoles (MB) [1].

	MB Inner Layer	MB Outer Layer
Strand		
Copper to superconductor ratio	1.65 ± 0.05	1.95 ± 0.05
Diameter after coating [mm]	1.065 ± 0.0025	0.825 ± 0.0025
Filament diameter [μm]	7	6
Number of filaments	~ 8900	~ 6500
Critical current [A] 10 T, 1.9 K 9 T, 1.9 K	≥ 515	≥ 380
Cables		
Number of strands	28	36
Cable dimension (at room temperature)		
Mid-thickness at 50 MPa [mm]	1.900 ± 0.006	1.480 ± 0.006
Thin edge [mm]	1.736	1.362
Thick edge [mm]	2.064	1.598
Width [mm]	15.10	15.10
Keystone angle [degree]	1.25 ± 0.05	0.90 ± 0.05
Critical current I_c [A] 10 T, 1.9 K 9 T, 1.9 K	> 13750	> 12960

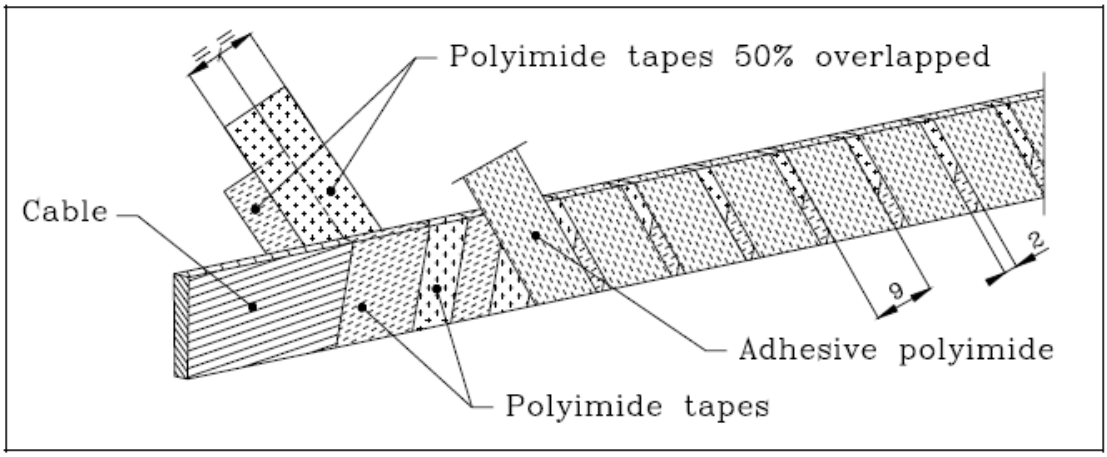

Fig.3.3.4: Insulation of the superconducting cable [1].

Between blocks of conductors the copper wedges are inserted to form appropriate curvature of the magnetic field lines and ensure a quasi-circular coil geometry. End spacers are insulating fillers, produced of epoxy impregnated fibreglass. They have been designed to constrain the conductor to a consistent and mechanically stable shape.

Induction of the 8.33 T magnetic field into the vacuum chamber allows to keep the 7 TeV proton beam on the orbit. Magnetic length of Main Dipoles is 14.3 m while overall length (with included ancillaries) is about 16,5 m.

3.4 Beam Loss Monitoring

Even the loss of very small fraction of the circulating beam may induce a quench of the superconducting magnets and even damage them. Therefore the detection of the particle loss must be performed. The LHC protection system generates a beam dump trigger when the losses exceed thresholds. Moreover it allows to investigate an orbit distortion, a beam oscillations and a particle diffusion.

Due to physical limits (inter alia: lack of space, distortion of magnetic field) it is impossible to place any conventional detector inside the cold mass. Therefore ionization chambers are located outside the magnet cryostat to detect the energy deposition of secondary particles. The Beam Loss Monitors (BLM) are 500 mm long cylinders with a diameter of 87 mm. Inner electrodes are separated by 5 mm. The chamber is filled with N_2.

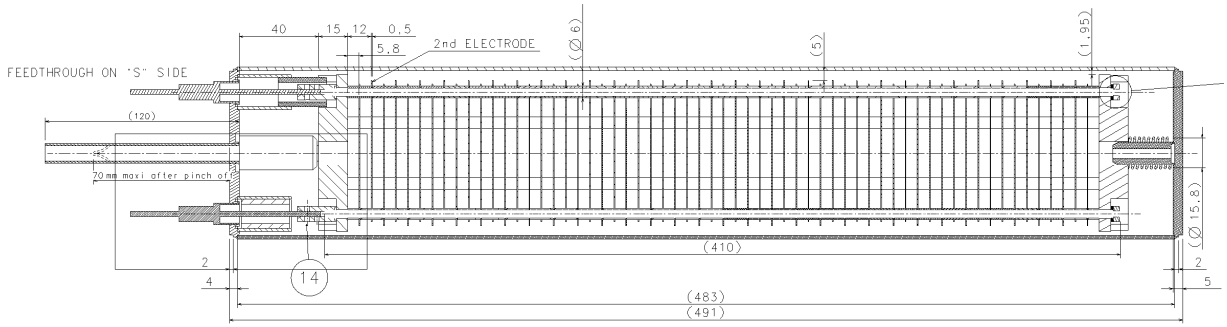

Fig. 3.4.1: BLM design. Part of the drawing no. LHCBLM__0001[2].

Fig. 3.4.2: Picture of the LHC BLM detector without the cover tube [7] .

Fig. 3.4.3: All LHC BLMs are painted yellow. One the picture: BLM mounted on Main Dipole.

Fig. 3.4.1 presents the technical design of BLM, while Fig. 3.4.2 - a picture of real detector. Fig.3.4.3 shows BLM mounted on the LHC Main Dipole.

There are about 4000 Beam Loss Monitors in the LHC ring which observe losses at the most likely locations.

Each detector has been tested during the Beam Time. It takes place in The North Area (see Fig.1.1) in Prevessin (French site). The beam is derived from the SPS with energy of 450 GeV and is aimed at a metal target. As a result of collision, the shower of secondary particles develops and finally can be measured by the Beam Loss Monitor. This method allows to do a calibration of every detector. Fig.3.4.4 presents steps of measurements. Left picture: sixteen detectors are placed in a wooden box; middle picture: a cabling is connected to detectors; right picture: the box with SEMs is located on a movable stage in the front of the target. In the case of BLMs, the procedure is more or less the same.

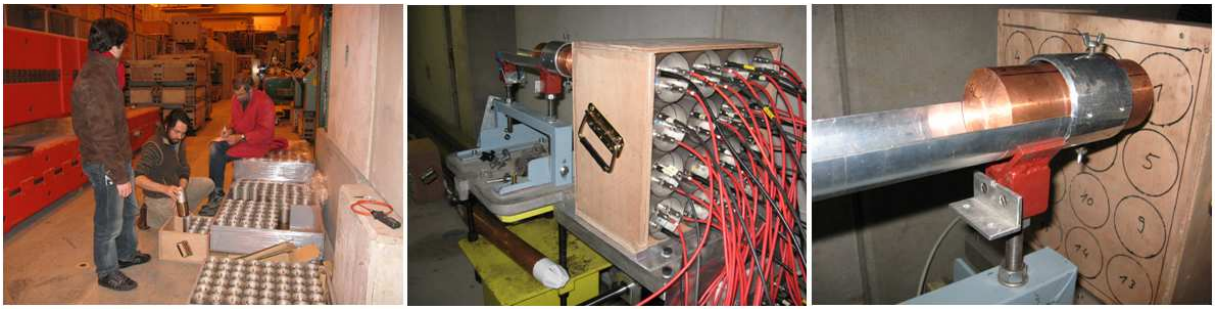

Fig.3.4.4: Testing the Secondary Emission Monitors (SEM). Description in the text.

4. Geant4 simulations

4.1 Motivation

It has already been mentioned the Large Hadron Collider is the most powerful accelerator ever constructed. The circulating beams with energy of 7 TeV bring not only opportunities of great discoveries but also wide range of new challenges in regard to a need of protection the superconducting magnets.

The most crucial components of the LHC magnets are coils, made of niobium-titanium cables and brought into superconducting state (1.9K). Because of that, they are more imperilled on damages – if the energy deposition exceeds a stability margin, sudden increase of temperature causes a phase transition, a part of superconductor is taken out from the superconducting state and therefore a sudden growth of resistance occurs.

These effects can lead to a permanent breakage of coils and must be prevented. Detectors which record signal of losses must be applied. Due to a lack of space inside the magnets, Beam Loss Monitors (BLM) have been mounted outside the cryostat. The goal of Geant4 simulations is to estimate correlation between energy deposition inside the coils and signal in BLMs.

4.2 Strategy

Fig. 4.2.1 shows the strategy of a preparation the Geant4 simulation. All information about geometry as well as drawings of Main Dipole have been derived from the LHC Design Report, The CERN Engineering & Equipment Management Service (edms) and CERN Drawing Directory Server (CDD). In regard to very sophisticated structure of MB some simplifications have been required (see Chapter 3.3). The magnetic field map has been obtained using ROXIE, a program for magnetic field calculations inside the magnets [5]. Then, after implementing an appropriate kind of physics (see Chapter 4.5), a system of measuring the energy losses (ROGeom, SensitiveDetector) and detectors, which score secondary particles outside the magnet (BLM, see Chapter 3.4), the simulations have been ready for running. Processes, which take place, have a probabilistic nature. Therefore the large number of events (in the order of 10^3) has been needed to reach the correct statistics.

Directly from the Geant4 simulation the energy deposition in coils and fluence of secondary particles reaching detectors have been obtained. Taking into account the quench level [6], one is able to count a critical number of protons. On the other hand an application

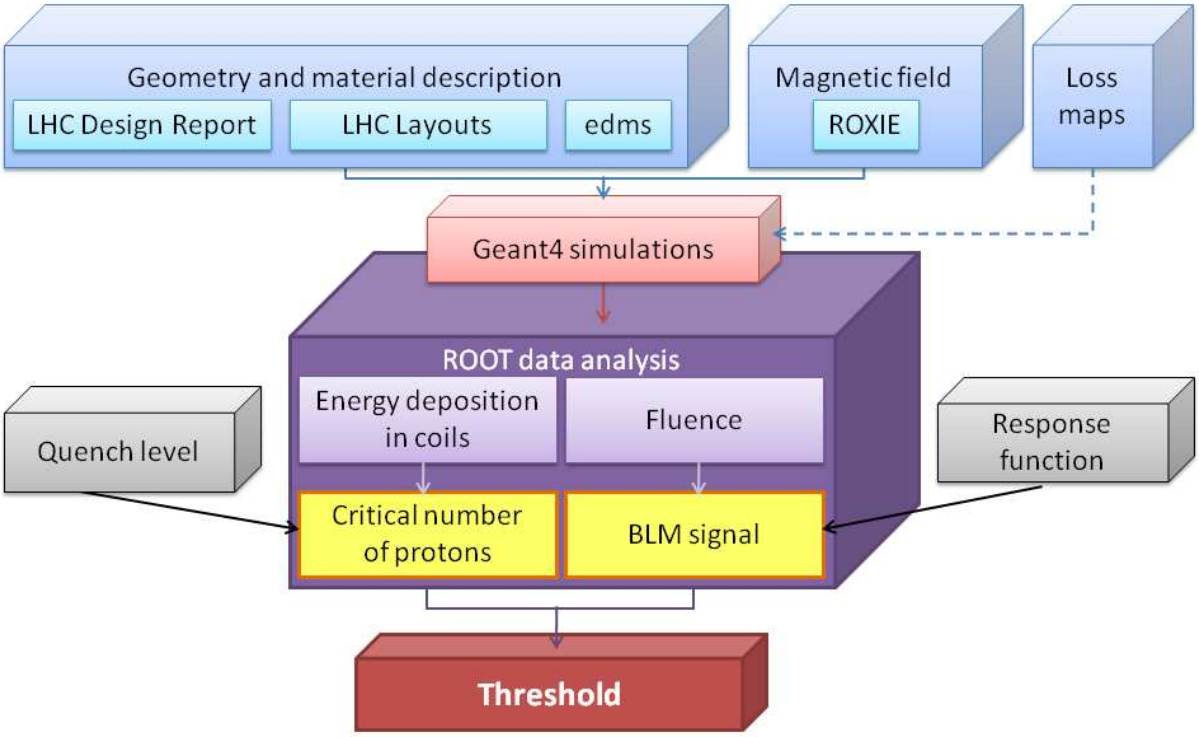

Fig. 4.2.1: Flowchart of the strategy.

a response function [7] allows to estimate the BLM signal. Knowing these two values the Main Dipole thresholds are quite-well defined – the correlation between the situation inside the magnet and the signal measured by detectors is specified.

4.3 Geant4

The Geant4 (GEometry ANd Tracking) is a sophisticated scientific tool for the high energy physics the simulations, using Monte Carlo methods. C++ based the Oriented Object programming is an characteristic for this platform.

Each program contains from several up to dozens of files: source files with ".cc" extension and include files with .hh. In the Tab.4.3.1 some of the files have been described.

It must be stressed that all files are strictly combined and lack of even one component can cause a faulty operation of the entire system.

Geant4 gives a possibility of investigations on the passage of particles through matter. Therefore is used for HEP, nuclear physics, medical, space and accelerator physics researches.

These simulation have been fully done in the Gent4 version 0.9 patch 01. It is worth to stress the fact that 282 physical volumes have been implemented to construct the Main Dipole geometry properly.

Table 4.3.1: Geant4 files

No.	File name	Main contents
1	MDBeamPipeHit.cc	Definition of values which are to be measured (ρ, φ, z, energy deposition etc)
2	MDBeamPipeROGeom.cc	Placement the read out geometry onto beam pipes (cold bores)
3	MDBeamPipeSD.cc	Division of beam pipes (cold bores) into cells
4	MDBeamScreenHit.cc	Definition of values which are to be measured (ρ, φ, z, energy deposition etc)
5	MDBeamScreenROGeom.cc	Placement the read out geometry onto beam screens
6	MDBeamScreenSD.cc	Division of beam screens into cells
7	MDCoilHit.cc	Definition of values which are to be measured (ρ, φ, z, energy deposition etc)
8	MDCoilROGeom.cc	Placement the read out geometry onto coils
9	MDCoilSD.cc	Division of coils into cells
10	MDDetectorConstruction.cc	Implementation the materials and the geometry of magnets
11	MDDetectorMessenger.cc	Magnetic field and detector management
12	MDEventAction.cc	Collection of information obtained by single cell (ρ, φ, z, energy deposition etc)
13	MDMagneticField.cc	Magnetic Map from ROXY
14	MDParameters.icc	Introduction the constant dimensions
15	MDPhysicsList.cc	Definition of particles and interactions between them
16	MDPrimaryGeneratorAction.cc	Primary number of particles, their coordinates, momentum direction and energy.
17	MDRunAction.cc	Definition an action at the beginning and the end of each run
18	MDSteppingAction.cc	Registration of particles entering the detector
19	MDSteppingVerbose.cc	Collection of units (length, energy etc.)
20	RootInterface.cc	Creation the ROOT files for an analysis

Lxbatch cluster at CERN has provided the performance of these simulations. An average simulation of one proton has taken approximately 30 minutes.

4.4 The Geometry

During the geometry implementation a compromise between estimated running time and an accuracy of introduced elements has had to be obtained.

On the one hand all major parts which comprise magnets had to be taken into account, on the other hand some simplifications have been required due to a magnet complexity.

Therefore, the cryostat, the thermal shield, the helium vessel, the iron yoke, collars, superconducting coils, cold bores and beam pipes have been implemented. Such elements as bus bars, instrumentation wires, heat exchanger pipes and alignment targets have been neglected because they are not in the way of considered particle losses. Also the concrete tunnel as well as the soil surrounding it have been simulated due to the sufficient role of neutron thermalization. Fig.4.4.1 presents a overall layout of the simulated space.

Summing up, a lot of importance has been attached mainly to these aspects which have a significant influence on creation, propagation and shape of the hadronic shower.

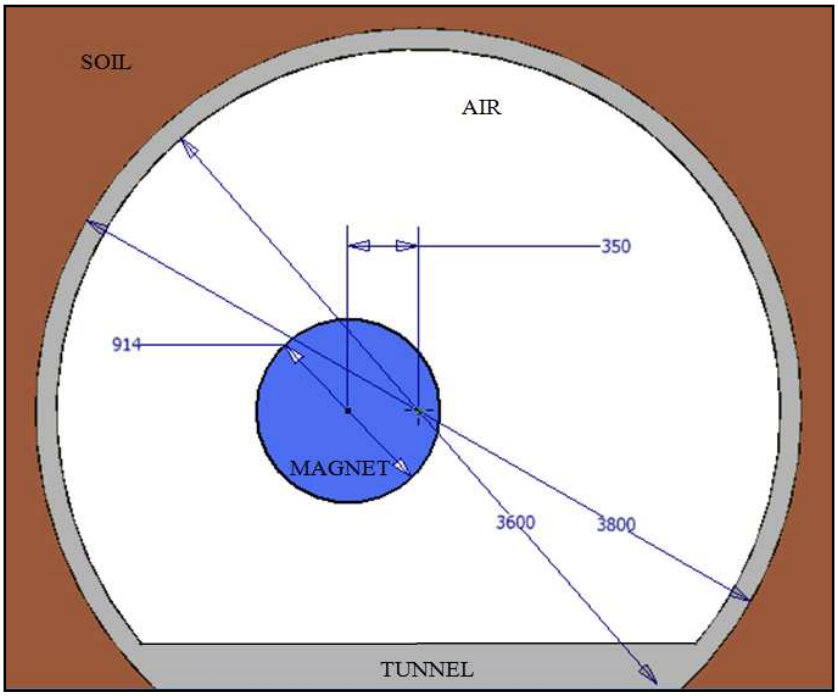

Fig.4.4.1: Overall layout of the simulated underground. It can be noticed that the magnet doesn't lay in the axis of the concrete tunnel.

4.4.1 Superconducting coils

In Geant4 simulation the superconducting coils have been implemented as it is shown on Fig. 4.4.1.1. A visualization of endings have been given on Fig. 4.4.1.2. Drawing of the Main Quadrupole has been shown to illustrate a curvature of coil endings.

The applied simplifications have been listed below:

- the material is homogenous. Instead of implementing each cable, each strand and each filament, four pieces of a uniform mater with the weighted density of niobium, titanium, copper and liquid helium have been introduced. Calculations have been made as presented in Appendix A.
- The left side of Fig.4.4.1.3 (a part of Drawing LHCMBPA_0001 ; Coil – Conductor Distribution) shows a construction of cables which form the coil. In Geant4 geometry a value of 5.69 mm has been neglected and an angle has been implemented as it's shown on Fig.4.4.1.4. An error is small - an excess from one side is countervailed by a reduction from the other side.
- Copper wedges which are normally mounted between cables have been neglected – these do not lay neither in horizontal not in vertical plane (see Chapter 4.9).
- An insulation of cables and around the coil has been omitted as it doesn't impact significantly on the creation of the hadronic shower.

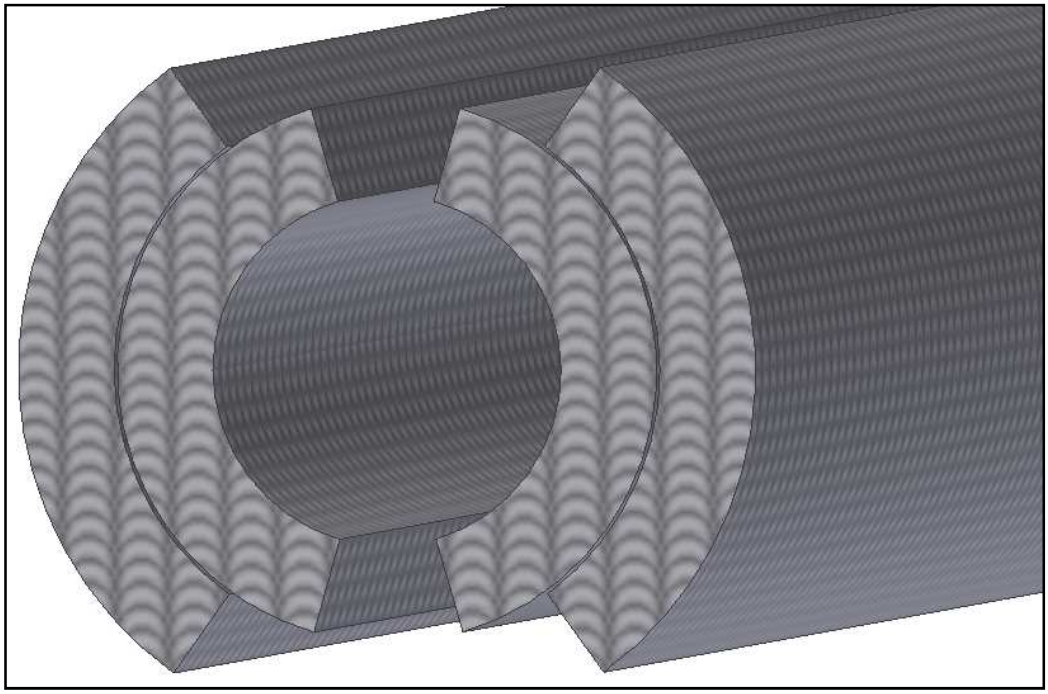

Fig.4.4.1.1: Visualization of Main Dipole superconducting coils which have been simulated in Geant4.

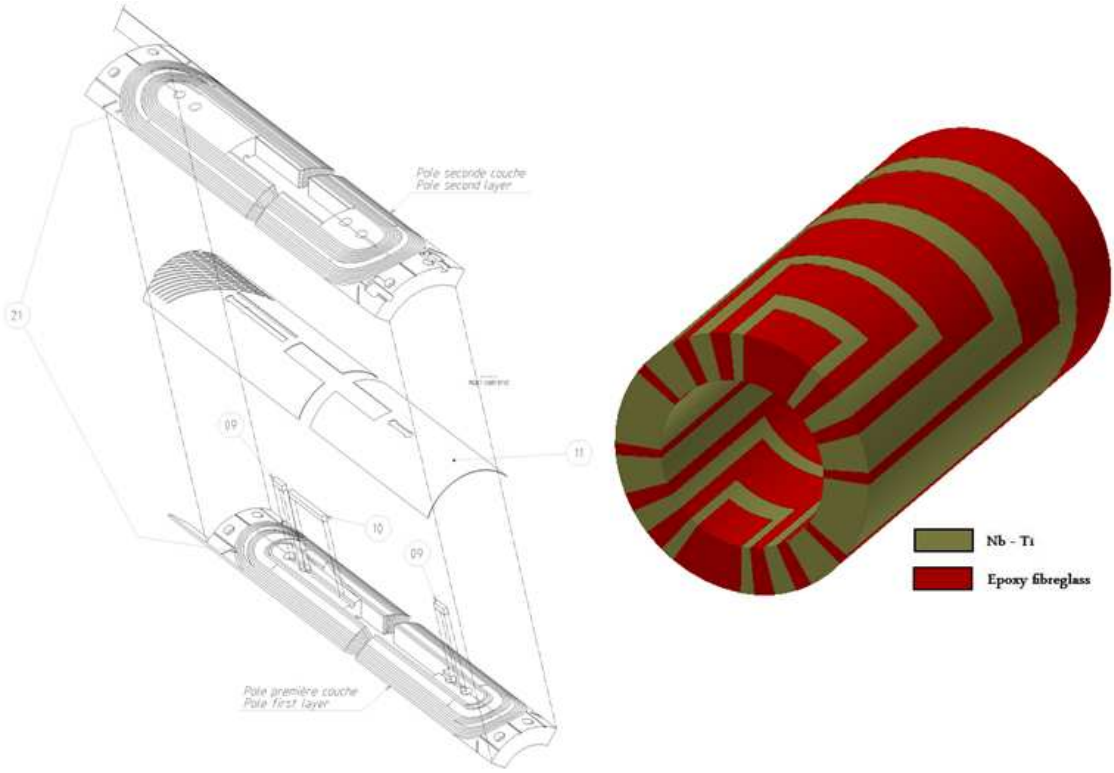

Fig.4.4.1.2: Endings of superconducting coils. On the left: technical design of MQ – LHCMQ_IS0015[2]; on the right: simulated geometry. Red colour corresponds to epoxy fibreglass fillings and olivine one to the niobium-titanium core.

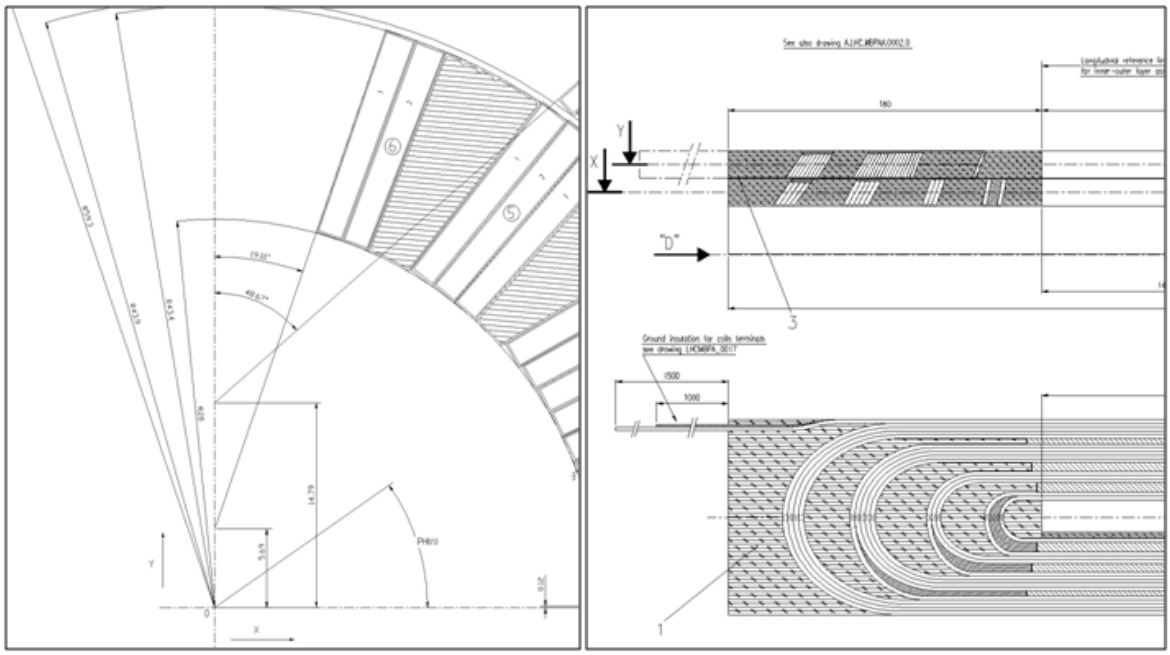

Fig.4.4.1.3: Design of the superconducting coil; left side: a part of the CDD drawing (LHCMBPA_0001); right side: a part of LHCMBPAA005[2] - cross-section of MB coil ending [2].

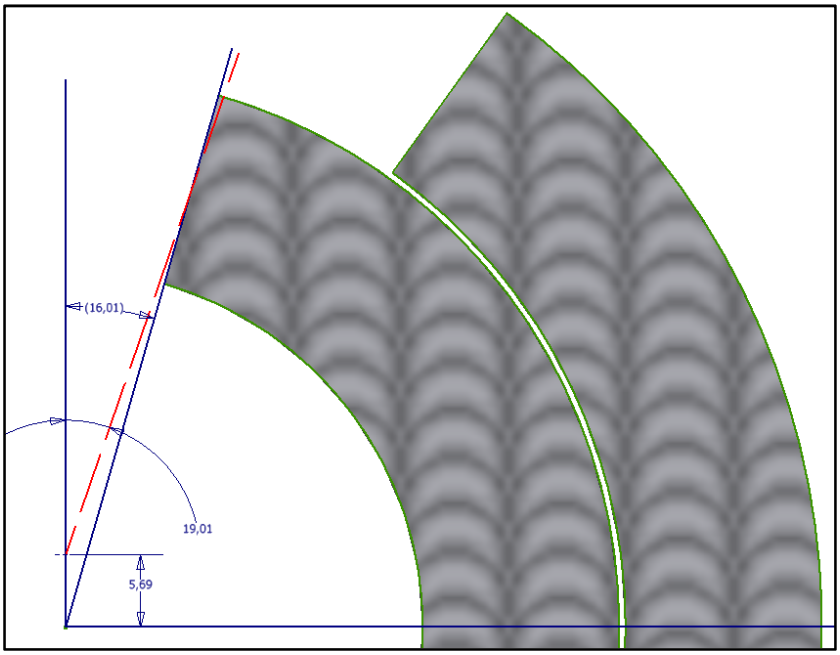

Fig.4.4.1.4: Simplifications applied during implementation the superconducting coils. Red dashed line points the original curve, blue one – applied in Geant4 simulation.

- A coil ends implementation is quite difficult due to a cables curvature. Finding an appropriate algorithm to create quasi-smooth and continuous geometry would extremely extend the running time. As it has been mentioned, the most important are the material amount and the density. Therefore, endings have been simplified as it is shown on the Fig.4.4.1.2. One can see that space between cables is now filled with the epoxy impregnated fibreglass (LHCMBPAA005) – the right side of Fig.4.4.1.3.

4.4.2 Beam Loss Monitoring

Beam Loss Monitors have been implemented as two cylinders with a diameter of 87 mm and a length even larger than the cryostat length. The reason of it has been to investigate the shape of the signal what is equivalent to the number of secondaries getting out of the magnet. Moreover this solution provides a flexibility of simulated cases – with regards to the LHC region, the monitors are located in different places on the magnet cryostat. This geometry impacts on particles scored by monitors – these ones which get the BLMs from end-caps are neglected. Angular distribution (see Chapter 6.2) shows that the most of particles enters detectors with large angles and because of that a margin of error is small.

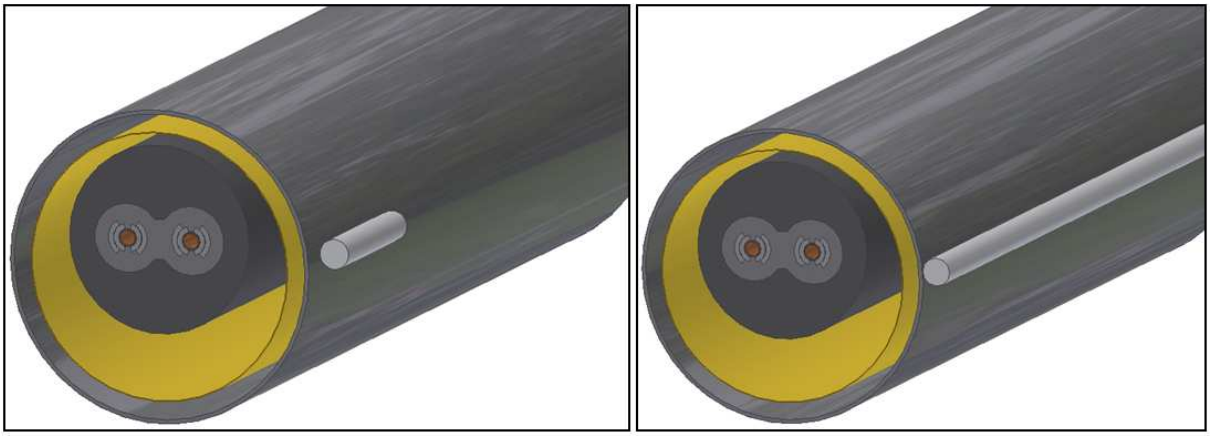

Fig. 4.4.2.1: Visualisation of BLM dimensions. On the left: the real BLM is a single detector outside the cryostat. On the right: in the simulation BLM has been implemented as a long tube all along the magnet.

The difference between the real case and the simulated one have been visualized on Fig. 4.4.2.1.

4.5 Physics

Geant4 gives an incredible wide range of choice the miscellaneous physical interactions between particles. In this study the list called QGSP_BERT_HP has been applied as regards to earlier comparisons which has been done in [7]. This list combines the Quark-Gluon String (QGSP) modelling of hadron interactions at energies above 12 GeV with the Bertini parameterization of the hadronic cascade below 10 GeV and with High Precision neutron transport (containing the resonant interactions with nucleai). From GEISHA the parameterized model on intermediate energy level (10-12 GeV) has been obtained.

The following particles have been considered:

- leptons: $e^-, e^+, \mu^+, \mu^-, \nu_e, \overline{\nu_e}, \nu_\mu, \overline{\nu_\mu}$
- mesons: $\pi^+, \pi^-, \pi^0, \eta, \eta', K^+, K^-, K^0, \overline{K^0}, K^0 - short, K^0 - long$
- baryons: $p^+, p^-, n^0, \overline{n^0}$

These undergo processes listed below:

- electromagnetic interactions:
  - → Compton scattering
  - → gamma conversion
  - → photoelectric effect
  - → multiple scattering

→ ionisation

→ Bremsstrahlung

→ annihilation

→ pair production

- hadron physics
- transportation

4.6 Readout geometry

The most fragile and sensitive components of LHC Main Dipoles are superconducting coils. Therefore, these simulations have been mainly focused on their protection.

Due to the larger exposition to secondary particles the inner superconducting coils have been investigated. As information about the energy deposition occurrence is substantial, both (left and right) coils have been divided into artificial cells (Fig.4.6.1). Each cell is approximately 47 mm long (z-division) with azimuthal size of 4° (phi-division). In the radial direction the coils have been divided into three parts (5.12 mm each). The bin size has been chosen to obtain an appropriate scale much smaller than the particle shower scale.

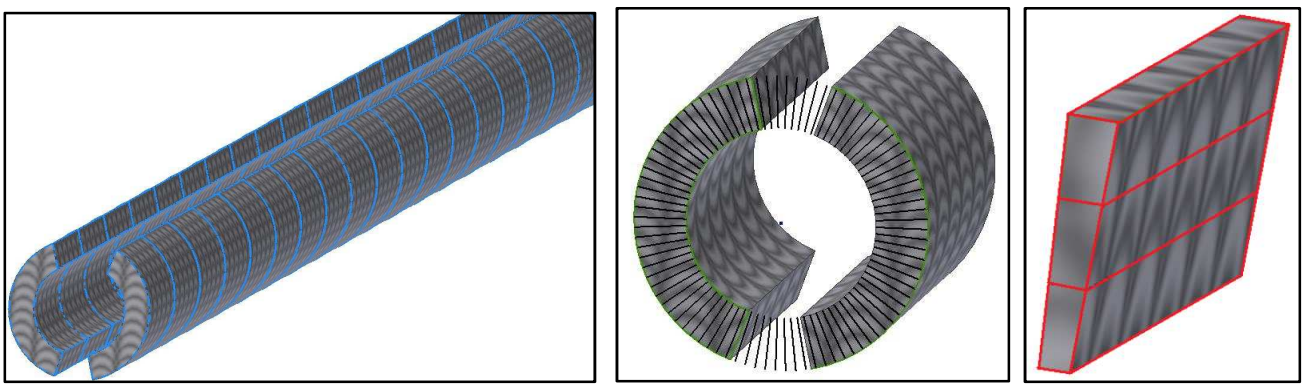

Fig.4.6.1: Each coil has been divided into 81 000 basic cells which register the energy deposition. Left plot: z-division into 300 pieces. Centre plot: φ-division into 90 pieces. Right plot: ρ-division into 3 parts.

4.7 Magnetic field

The magnetic field map has been implemented as an array of points with a mesh step of 5.1 mm obtained from the ROXIE (The **R**outine for the **O**ptimization of Magnet **X**-Sections,

Inverse Problem Solving and **E**nd Region Design) [5]. Between mesh points a linear interpolation of field values has been applied.

This is a 2D map. In a longitudinal plane, the magnetic field must smoothly go to zero, otherwise unphysical effect appear (Fig.4.7.1).

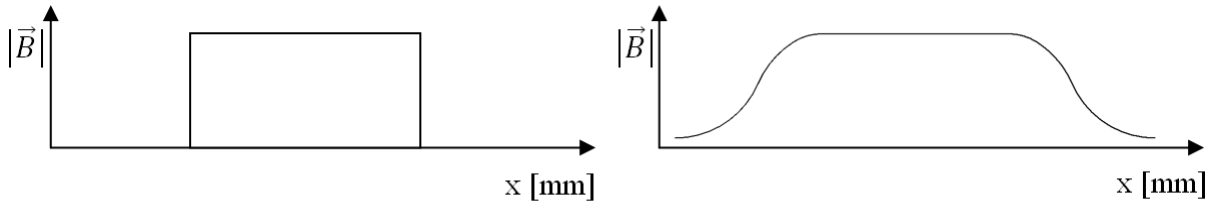

Fig.4.7.1: The magnetic field does not end sharply as it is shown on the left. The smooth, physically proper transition is presented on the right.

The field map inside the yoke is presented on Fig4.7.2. The coloured area corresponds to the iron yoke and arrows indicates directions of $\vec{B}$. Along the coil axes, in the centres of beam screens, the magnetic field is perpendicular to the motion of particles (the Lorentz Force Law). The field inside the coil is depicted on Fig.4.7.3.

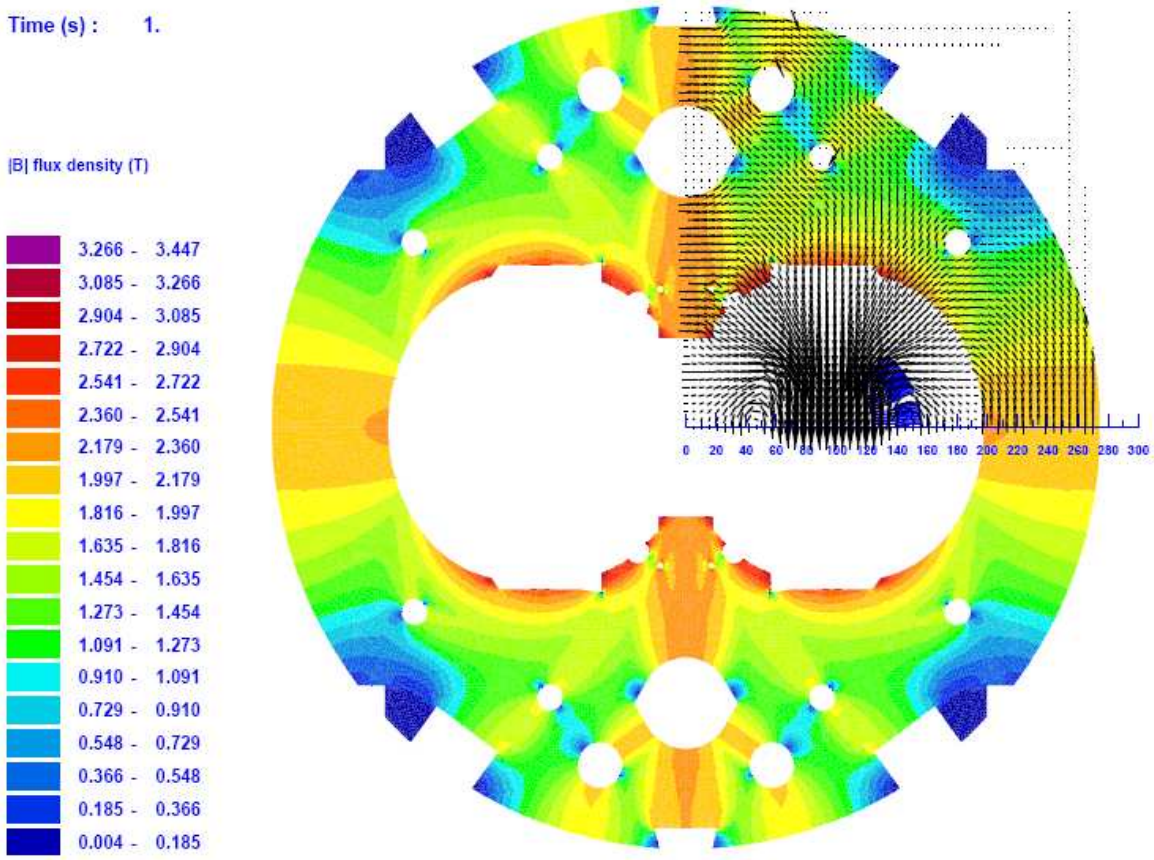

Fig.4.7.2: Magnetic field map of Main Dipole at 7 TeV. Arrows represent the vector of magnetic field [4].

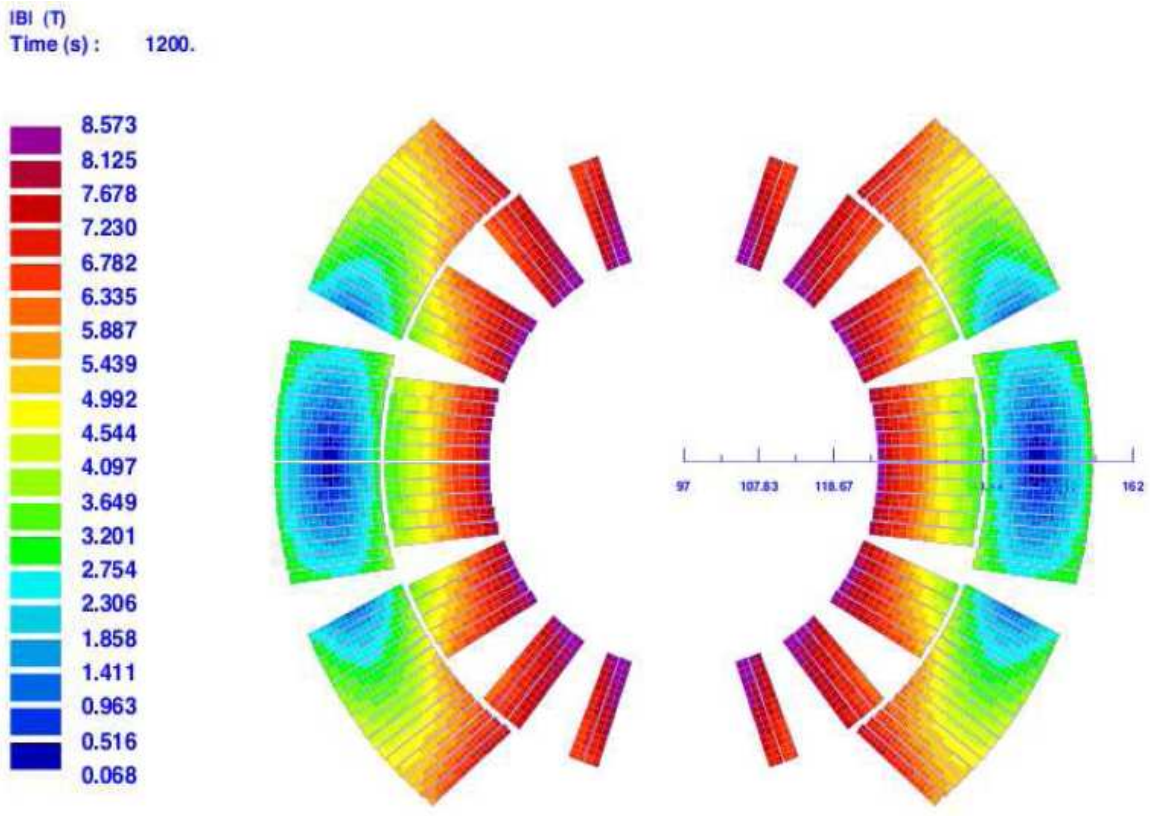

Fig.4.7.3: The map of magnetic field inside the coil. Collision energy considered [4].

4.8 Threshold

As it has been already mentioned (see Chapter 2.5), the superconducting coils can quench due to the energy deposition. The maximum value of E_{dep}, which does not cause the transition into the normal conducting state, is called the stability margin.

The beam abort thresholds in the Beam Loss Monitors are specified as they correspond to an increase of the quench-provoking temperature. The thresholds depend on three parameters:

- beam energy
- loss duration
- loss dimension.

In this study only fast transient losses have been considered, which means that a dissipation of energy does not occur outside the superconducting cables and the stability margin is defined by the enthalpy of the copper and the superconductor.

As the specific heat of the niobium-titanium strongly depends on magnetic field, it is different in various parts of superconducting cables.

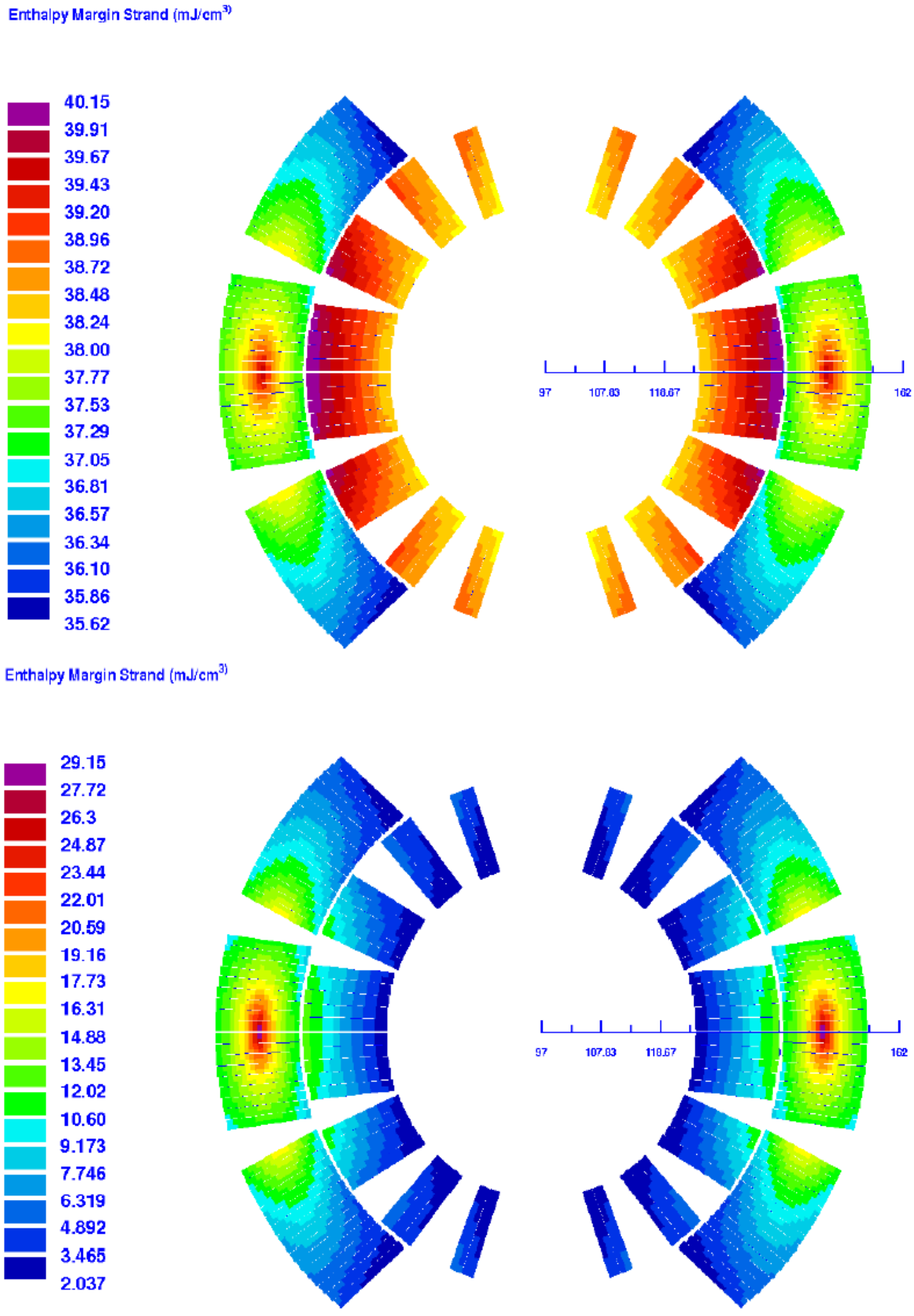

Fig.4.8.1: The transverse cross-section of the MB coil. The colour map represents a distribution of the quench margin. Upper plot: for injection current; bottom plot: for collision current. Courtesy [17].

A comparison of initial [14] and refined [6] calculations of the LHC dipole the cable enthalpy has been shown in Tab.4.8. Results of ROXIE [5] calculations has been presented on Fig.4.8.1.

Table 4.8: Comparison of cable enthalpy.

Source	Injection energy (450 GeV)	Collision energy (7 TeV)	Remarks
[14]	38 mJ/cm^3	0.8 mJ/cm^3	-
[6]	31.3 mJ/cm^3	0.93 mJ/cm^3	Cu/SC ratio, a presence of He and insulations have been taken into account

4.9 Loss locations

Three loss locations have been simulated – two horizontal (left and right) and one vertical (Fig.4.9.1). Despite the whole Main Dipole geometry (including end plates and interconnections) have been implemented, only the losses within the magnet length have been analysed.

In the High Energy Physics the statistics plays a crucial role. Therefore, for the injection energy 2000 protons have been used to simulate beam losses while for the collision energy the number of 1000 has been sufficient.

The energy range of considered losses varies from 250 GeV up to 8 TeV.

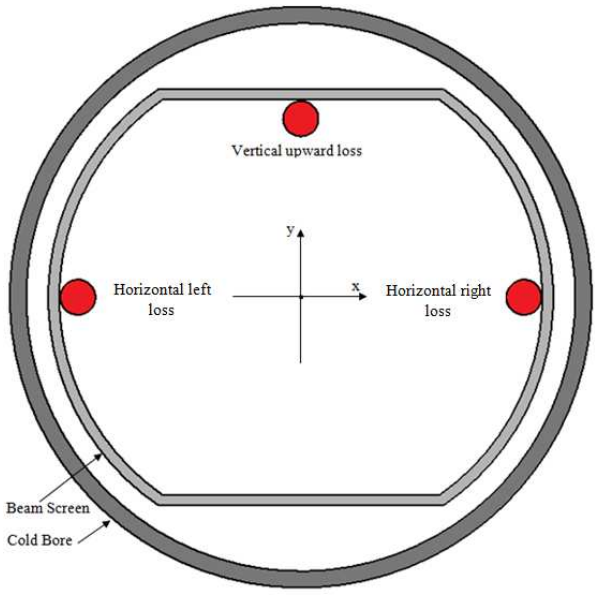

Fig.4.9.1: Three loss locations have been analysed.

5. Data analysis – the coils

Pointlike losses have been simulated, which means that the protons were hitting the beam screen in the same place (see Chapter 4.9). Further, the distribution of events is obtained by a convolution of pointlike losses with a broad gauss distribution - its width is dependent on the impacting angle (either 240 μrad or 750 μrad) and the beam intensity. The Gaussian along the beam screen (Fig.5.1) is a reflection of the loss distribution profile.

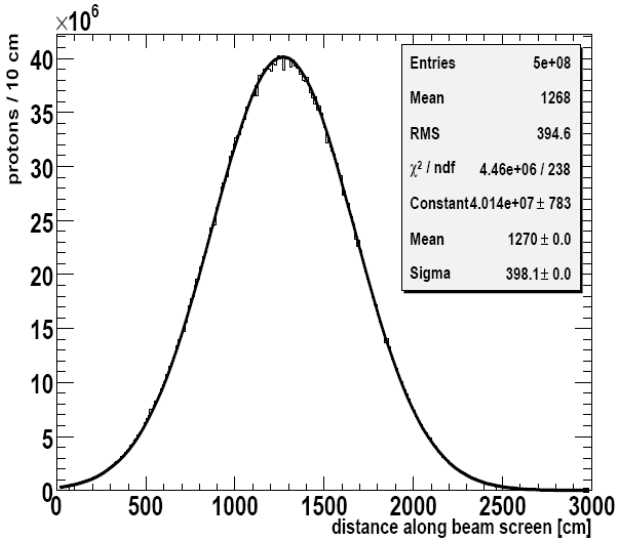

Fig.5.1: Lost protons distribution along the beam screen; simulated bunch contains $4 \cdot 10^9$ protons, transverse σ_{beam}=1mm [4].

A magnitude of thresholds varies according to the loss width. If the losses are more localized, the threshold is lower and analogically – the higher threshold is induced by the wider losses.

5.1 Deposition of energy in the coil

Initially the hadronic cascade develops in the beam screen, spreads through the cold bore and finally deposits a part of its energy in the magnet coils. Of course, deposition of energy appears in every element which stands on the way of the propagating particle shower but only the superconducting coils are critical due to quenching. A pie chart on Fig.5.1.1 depicts an estimated contributions of the cold mass ingredients to release the energy.

A “slice” (see Chapter 4.6) of the geometrical coil with a width of one cell in z-direction (a left plot of Fig.5.1.1) is presented on Fig.5.1.2. This “slice” represents the most exposed part of the magnet. The energy density (E_D) distribution in given by a colour map and reaches the highest values in the beam screen and the cold bore.

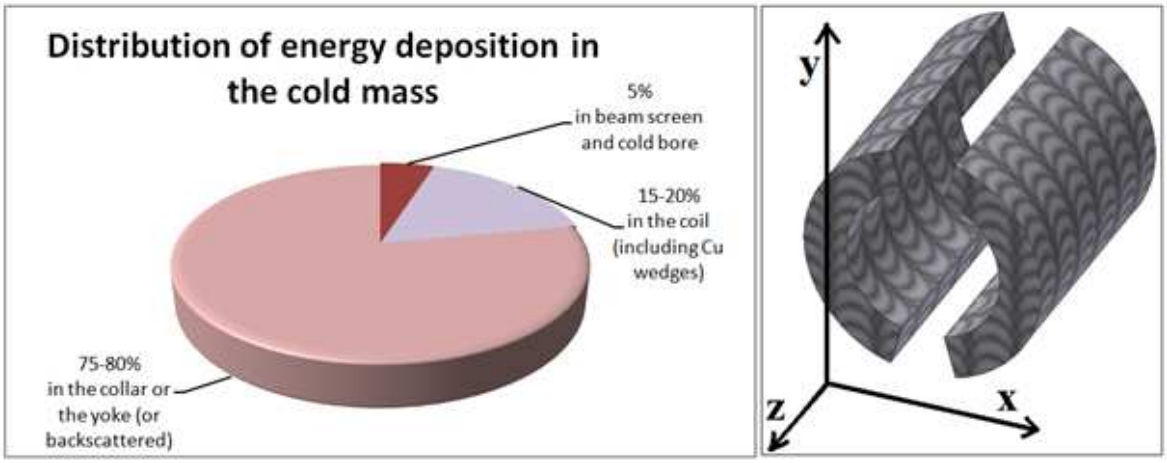

Fig.5.1.1:Left plot: Energy releases appear on the each stage of cold mass; right plot: the coil orientation in the Gean4 coordinate system.

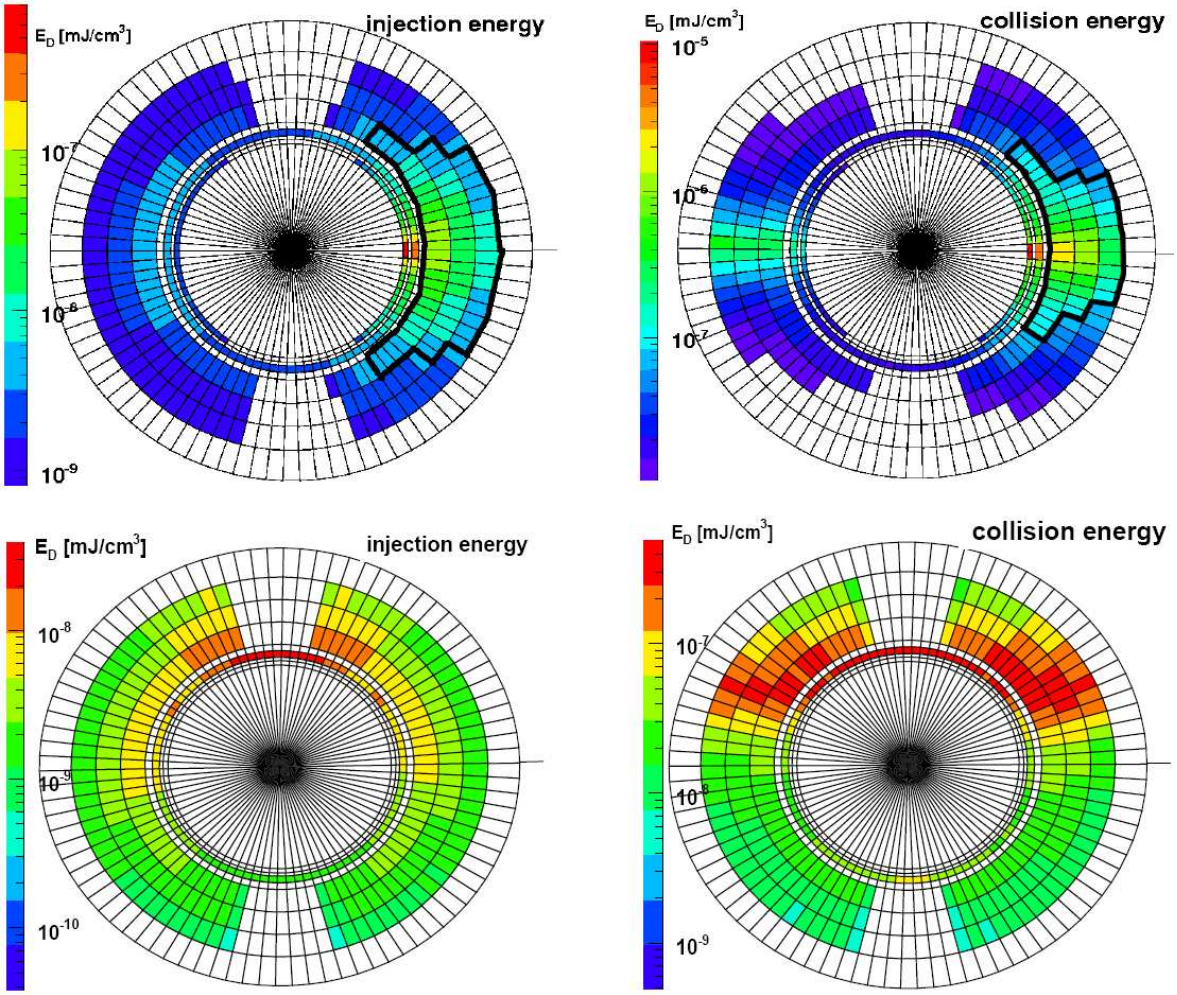

Fig.5.1.2: Cross-section of coils where the energy deposition for injection (450 GeV) and collision (7 TeV) beams reaches the maximum values[4]; top plots: horizontal losses; bottom plots: vertical losses, description in the text.

A higher magnetic field (at collision energy of 7 TeV) results in a lower vertical and higher horizontal spread of energy – the energy is concentrated in horizontal plane. A thick black curve has been drawn around a region which contains 90% of the total energy deposited in the right coil. The region of 7 TeV-case is made of 46 cells (40% of entire "slice" of the coil). In contrast, for the case of 450 GeV, the region expands to 63 cells (40%).

While considering the vertical losses (bottom plots of Fig.5.1.2), one can notice that the magnetic field shifts the direction of cascade up to 60 degree (an appearance of the particle cascade peak) from original direction. This effect is favourable from thermal point of view because the fragile external cables of the coils are less affected by losses. In case of injection energy the main part of energy is deposited outside the coils so the influence of the cascade development is irrelevant.

Fig.5.1.3 shows four configurations of the loss locations and the beam energies. The energy density for the most exposed azimuth of the coil is presented as a function of

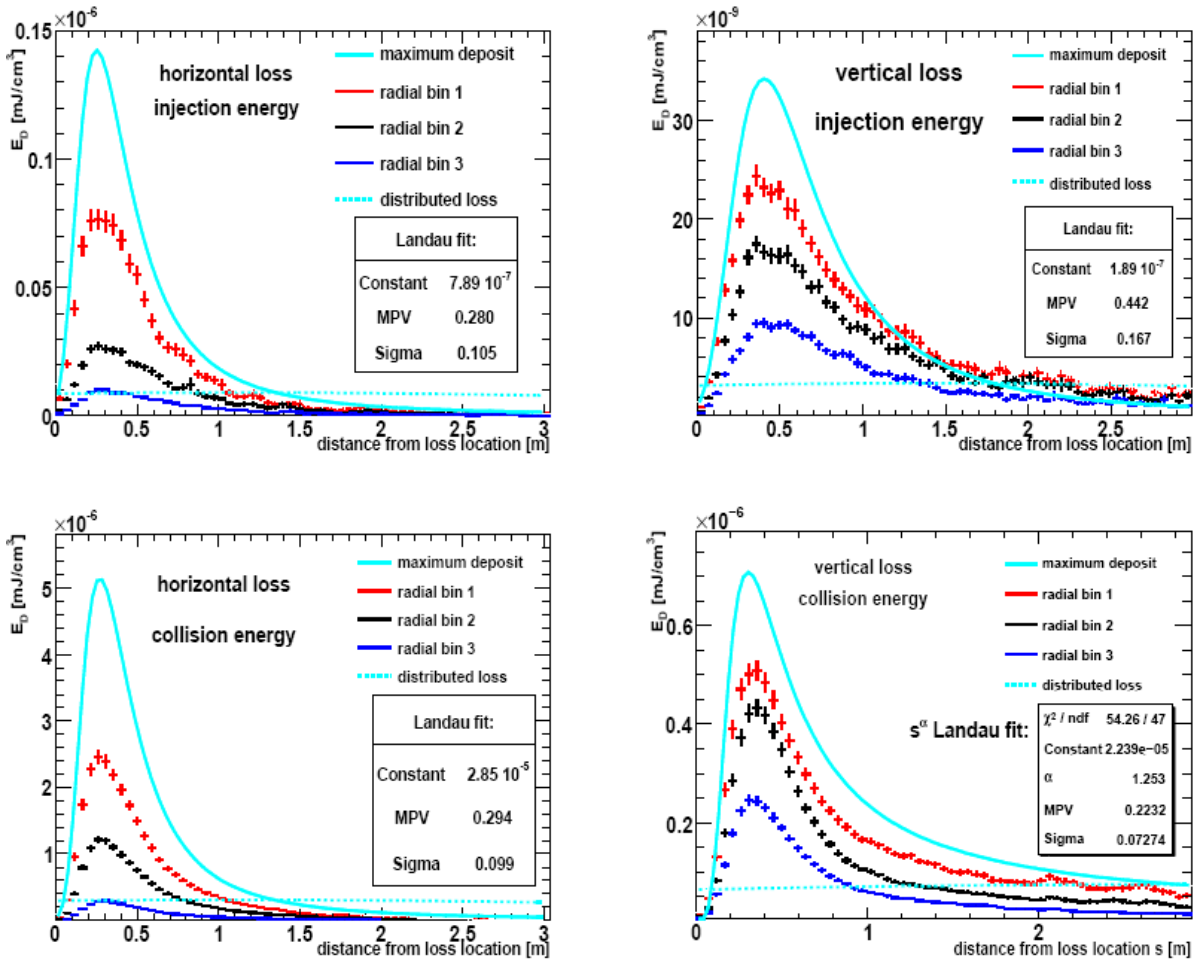

Fig.5.1.3: Longitudinal energy deposition in three layers of the coil. The bright turquoise continuous line estimates the maximum energy on the inner surface of the coil and is described by the Landau fit. The bright blue dashed line points the expected energy deposition in case of distributed loss [4].

longitudinal (z-direction) distance from the loss location. The red crosses correspond to the inner layer of bins, black ones to the middle layer and blue ones to the outer layer. In theses layers energy releases are defined.

The maximum of approximately $8 \cdot 10^{-8}$ mJ/cm^3 per impacting proton appears for the inner layer of the coil (red crosses) at about 0,35 m from the loss location in case of the injection energy. It is worth to stress that for the vertical loss the maximum value is three times smaller than in case of the horizontal loss. This fact results from a lack of superconductor in the vertical direction.

In case of collision energy the position of a peak remains the same but the maximum value increases roughly 31 times for the horizontal direction of the loss and 20 times for the vertical one .

5.2 Density of energy as a function of radius

On the inner plane of the coil the energy deposition (E_D^{max}) reaches the maximum. This value is derived from the radial dependence of the energy density (see Chapter 5.1). An exponent or a power law can be used to fit to the radial dependence. Thus, a value of the function at the inner radius of the coil is defined. An applied method is alike that one which is presented in [14].

The maximum energy is plotted on Fig.5.2.1. Beginning from the left, points correspond respectively to E_D^{max} in the beam screen, the cold bore and in three layers of the coil. The power law function $E_D = p_0(r - p_1)^{p_2}$ has been applied for the case of the injection energy. The calculations give the exponent value equals 2.40 while [14] reports 1.76.

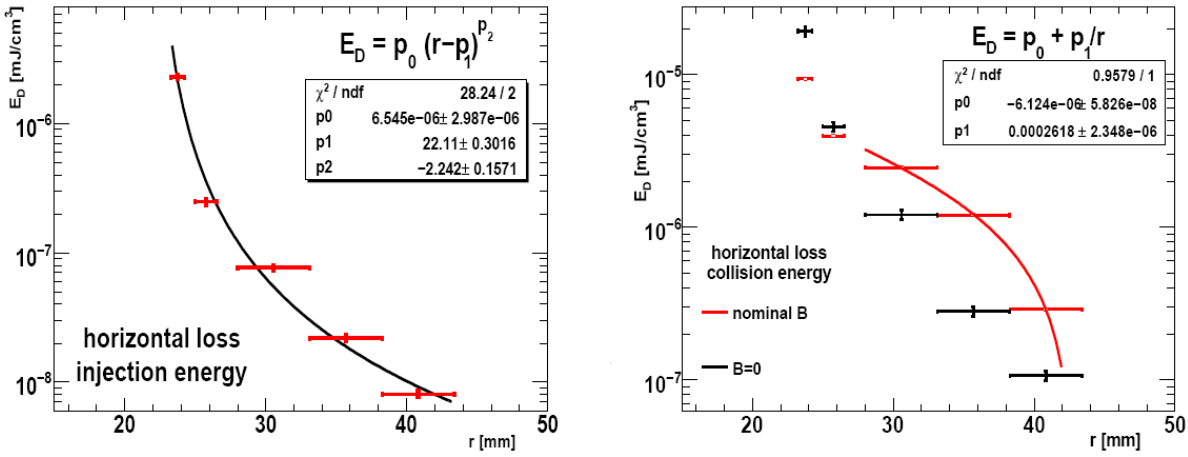

Fig.5.2.1: Maximum energy density along the most exposed azimuth; left plot: the injection energy and the horizontal loss; right plot: the collision energy; description in the text [4].

The shape of the transverse energy distribution is modified by the magnetic field at the high beam energy (right part of Fig.5.2.1). Two distributions are shown – red one refers to the situation with the magnetic field and black one to the situation without magnetic field. At high energies, what means also high magnetic fields, the simulated points do not match to the power law function in the entire range. A concentration of energy in the coil can be seen due to an influence of the magnetic field. At the same time, the deposition in the beam screen and in the cold bore is significantly smaller when comparing to results derived from simulations where magnetic field has not been implemented.

The Table 5.2.1 contains a comparison of p_2 factors estimated from this study and the report [14].

Table 5.2.1: Comparison of p_2 factors.

No.	Energy	Exponent value p_2	
		Geant4	Report [14]
1	Injection	2.40	1.76
2	Collision (B=0)	3.25	1.15

Analogically to the action made in 5.1, the 90% region has been estimated – 90% of the energy deposition takes place in 68 cells in case of the magnetic field absence and in 46 when the magnetic field is present.

Table 5.2.2 includes a juxtaposition of four scenarios .The ratios of the maximum energy deposition to the energy deposition in the inner layer have been shown. The $\frac{E_D^{max}}{E_D^{in}}$ ratio rises up with the beam energy what is implied by the influence of the magnetic field onto the hadronic cascade concentration.

Table 5.2.2: An influence of beam energy and loss direction onE_D^{max} to E_D^{in} ratios.

No.	Energy	Loss direction	$\frac{E_D^{max}}{E_D^{in}}$	
			in the peak (l = l_{peak})	in the tail of cascade (l = 2m)
1	450 GeV (injection)	horizontal	1.8	1.4
2		vertical	1.3	1.1
3	7 TeV (collision)	horizontal	2.3	1.5
4		vertical	1.4	1.2

6. Data analysis – the Beam Loss Monitors

It has been already highlighted in Chapter 4.2 that the fluence of secondary particles gets out of the magnet cryostat and results in the Beam Loss Monitor signal. Convolution of the fluence with an appropriate BLM response function gives finally the signal of the detector. The choice of the response function is based on an angular distribution of secondaries.

6.1 Register of the secondary particles by the detector

When hadronic shower exits the magnet, it reaches the volume of the detector (see Chapter 4.4.2). On each side of the Main Dipole the Beam Loss Monitor is placed (Fig.6.1.1). Right BLM originally surveys on the beam 1 but can also see an influence of the beam 2 (so-called cross-talk; see Chapter 2.6). The red histogram on Fig.6.1.2 corresponds to proper beam and blue one to the cross-talk from beam 2. On the top plots the results for the injection energy (450 GeV) have been shown and on the bottom ones – for the collision energy (7 TeV).

Table 6.1 contains a percentage contribution of the crosstalk into the BLM signal. An astonishing conclusion is that for the injection energy the impact of the crosstalk is more significant in case of the vertical loss direction while opposite for the collision energy.

It is worth to stress that in all studied cases the maximum of the fluence distribution appears about 1 m from the loss location.

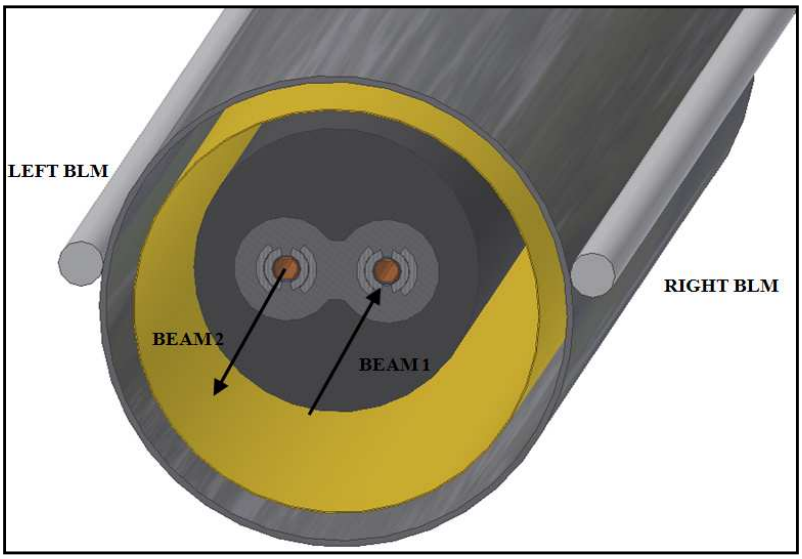

Fig.6.1.1: Two detectors record secondary particles coming from the clockwise beam and the counter-clockwise beam. Originally the right BLM surveys the beam 1 and left BLM observes beam 2 but the cross-talk also occurs.

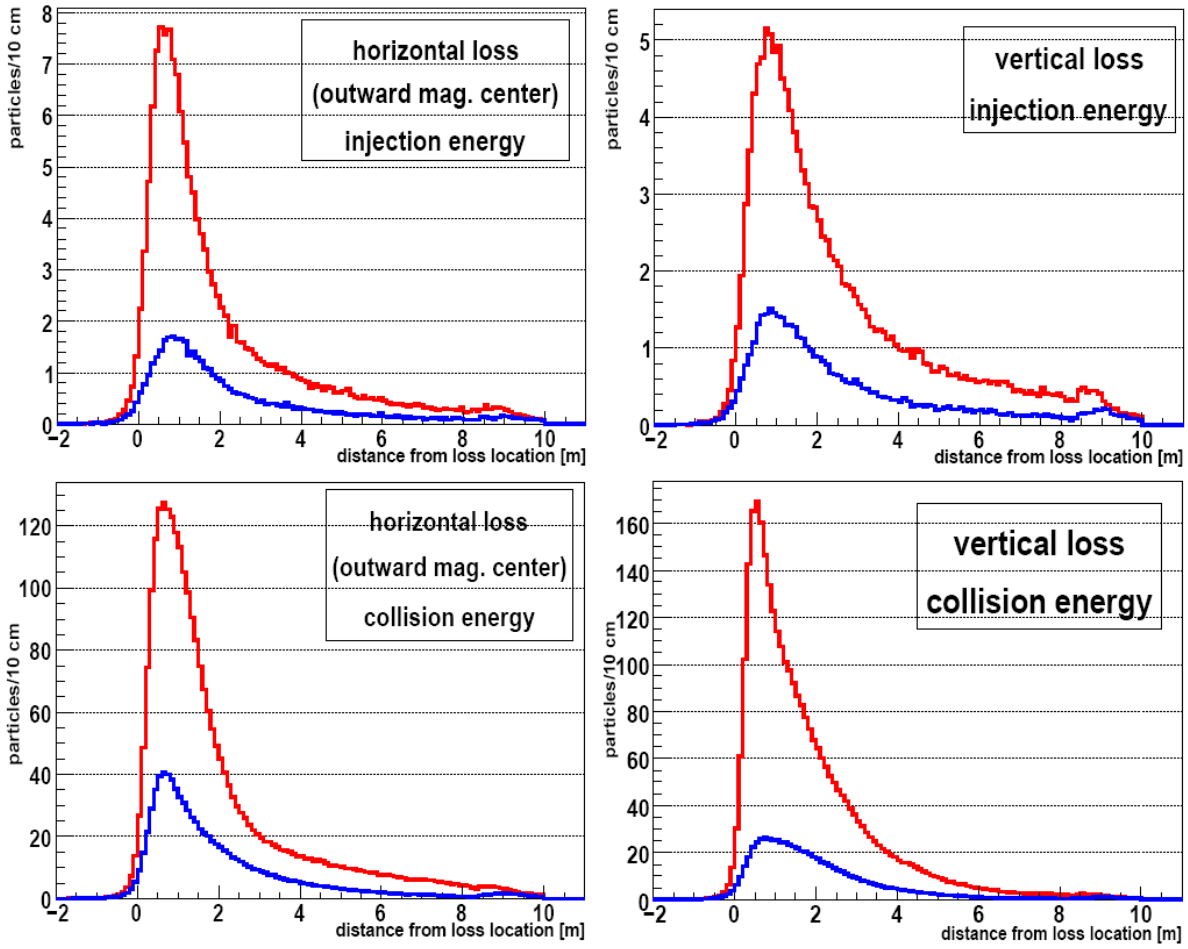

Fig.6.1.2: Multiplicity of particles outside the dipole cryostat in the direction of the beam loss (the red histogram) and in the opposite direction – crosstalk (blue histogram). Left top plot: injection energy, horizontal loss (outward magnet centre); right top plot: injection energy, vertical loss; Left bottom plot: collision energy, horizontal loss (outward magnet centre); right bottom plot: collision energy, vertical loss[4].

Table 6.1: Contribution of crosstalk into BLM signal

No.	Energy	Loss direction	$\frac{Signal\ in\ BLM2}{Signal\ in\ BLM1}$
1	450 GeV (injection)	horizontal	~ 22 %
2		vertical	~ 30 %
3	7 TeV (collision)	horizontal	~ 30 %
4		vertical	~ 15 %

6.2 Angular distribution

Secondary particles exit the magnet and enter the detectors. Each of them has its own momentum. Thus, the angular distribution is derived from the following equations:

$$\alpha = asin\left(\frac{p_t}{p_{total}}\right), \tag{6.1}$$

where

$$p_{total} = |\vec{p}_{total}| = \sqrt{p_x^2 + p_y^2 + p_z^2} \tag{6.2}$$

and p_t is the transverse momentum given by

$$p_t = |\vec{p}_t| = \sqrt{p_x^2 + p_y^2} \tag{6.3}$$

The results have been shown of Fig.6.2.1.

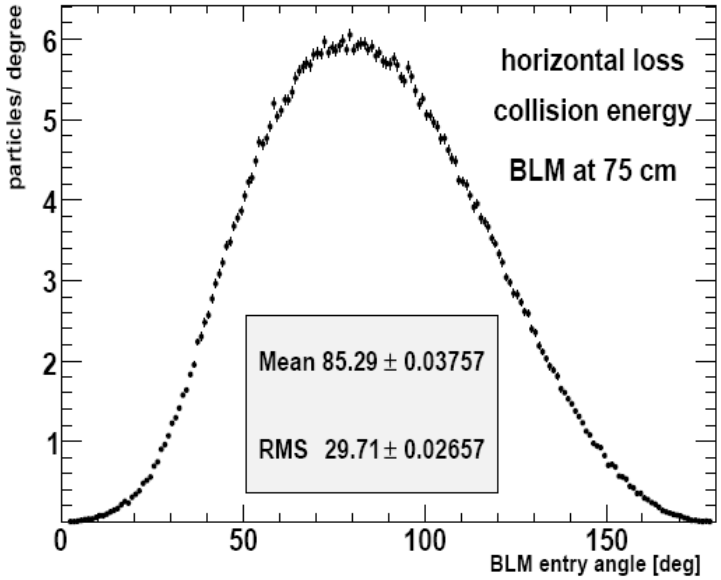

Fig.6.2.1 The angular distribution of secondary particles which enters the BLM at 75 cm from the loss location. The majority reaches the detector volume with almost a right angle. Therefore the end caps of BLMs can be neglected in simulations [4].

The most of trajectories of particles is perpendicular to the BLM longitudinal axis. By the way one can notice that a margin of error due to the implementation the continuous registering tube along the magnet (end caps skipped) is relatively small.

6.3 Spectrum of secondary particles

A wide range of miscellaneous particles is registered by Beam Loss Monitors. Neutrons and gammas give the dominant contributions to the total fluence – which is in agreement with the theoretical background (see Chapter 2.1). Fig 6.3.1 presents the spectra of

particles hitting the detector. The distance of measurement has been chosen to be 75 cm after the loss location. The peak of the spectrum reaches about 0.3 MeV regardless of the energy (the injection, the collision) which has been considered. Comparison of energies shows that protons and pions distinguishes among other ingredients of spectra. The same results as on Fig.6.3.1 but in differential fluence is shown on Fig.6.3.2. Here the distinct deviation from the power law can be observed for photons and neutron.

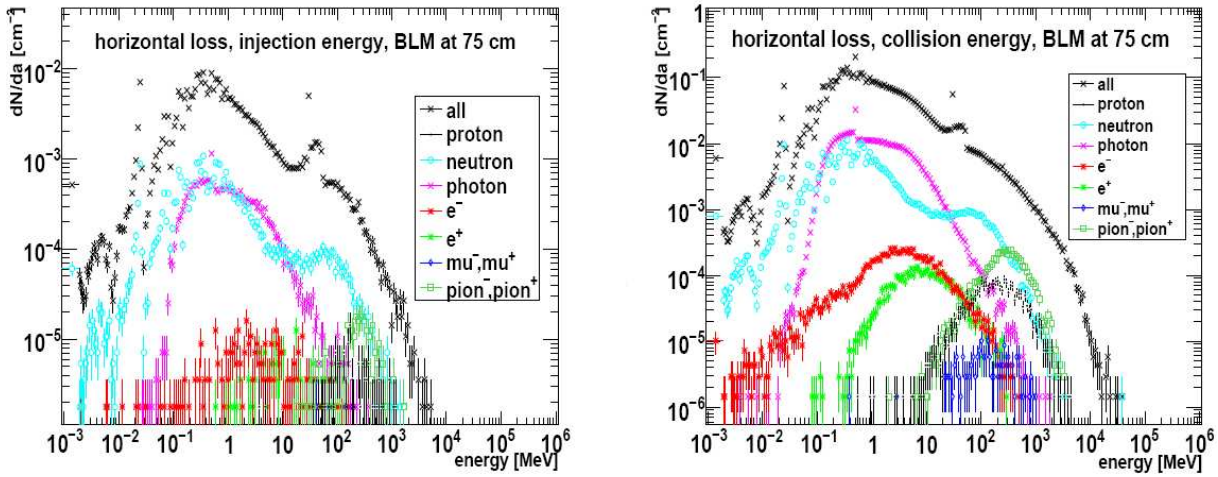

Fig. 6.3.1: Spectra of secondary particles for injection (left plot) and collision (right plot) energies. dN/da means the fluence of particles per primary impacting proton which enters the BLM 75 cm from the loss location. Beam 1 is considered [4].

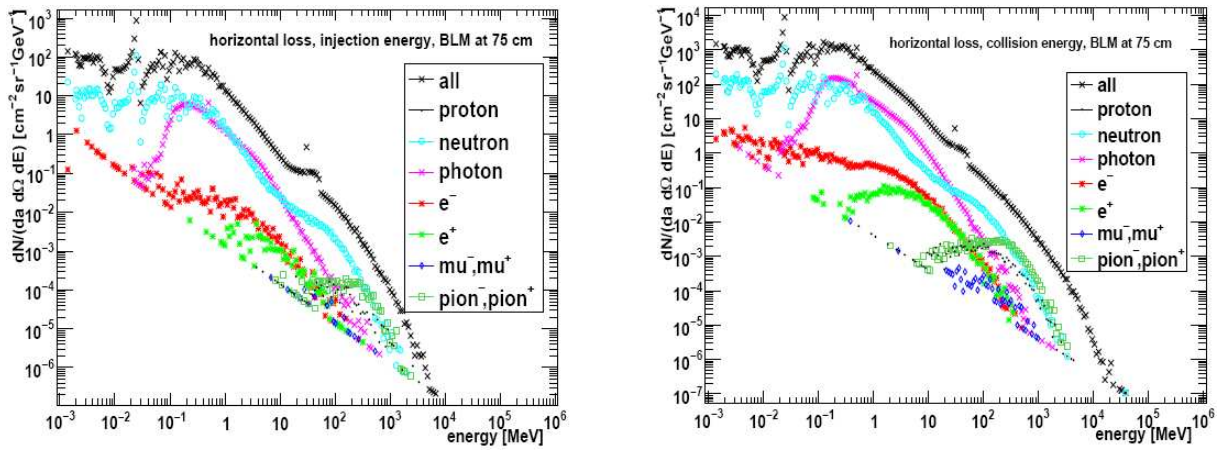

Fig.6.3.2: Differential spectra [4].

6.4 BLM signal

Pure spectrum of secondary particles registered by BLM is insufficient to determine a signal in a particular detector. The folding of the BLM response function must be applied (see Chapter 4.2). Detailed studies as regards of the ionisation chamber geometry (see

Fig.3.4.2) and an angle of impacting shower has been done in [7] and the folding procedure is described by the equation:

$$Q = \sum_{i=1}^{m=4} \left(w_i \cdot \sum_{j=p,n,e^-,\gamma\ldots} \sum_{k} R_{ijk} N_{jk} \right) \tag{6.4}$$

Four angles of incidence have been taken into account: 0°, 30°, 60°, 90° (see Fig.6.4.1). Thus the first sum in the equation is over these response functions. For the zero angle and the right angle functions the small tilt has been provided due to simulation artefacts. The weights w_i correspond to a population of particles in the angular bins and are multiplied by the fluence of particles folded with the response functions. Final sum is over the binning of the fluence and response function histograms. Angular bins are shown on Fig.6.4.2 as dashed steps.

Fig. 6.4.2 shows the design of ionisation chamber – it can be easily deduced that only the area between electrodes is active (38 cm). Thus the convoluted spectrum of particles outside the magnet is multiplied by 0.76 (the considered in simulations BLMs are 50-cm long).

A procedure of the signal calculation is shown step-by-step. Beginning from Fig.6.4.3, the energy input of each kind of particles to the total detector signal is simulated (plots on the left) and then the results are integrated (plots on the right). In respect to the response function shape, the contribution of specific particles can change. For example the impact of neutron on the detector signal decreases while protons and pions start to dominate due to their peaks in a particular range of energy.

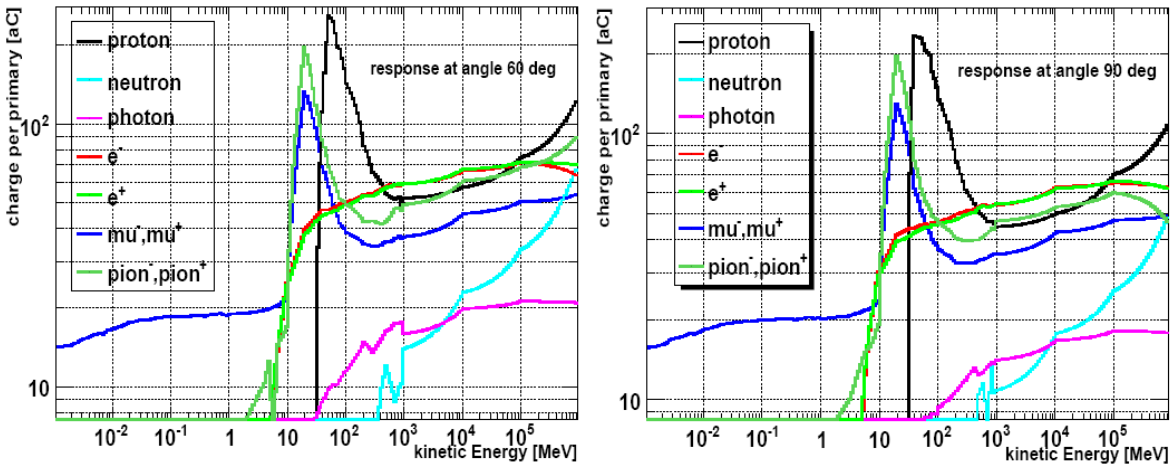

Fig.6.4.1: Comparison of two response functions [7]; left plot presents 60 degree response function and right one - 90 degree response function.

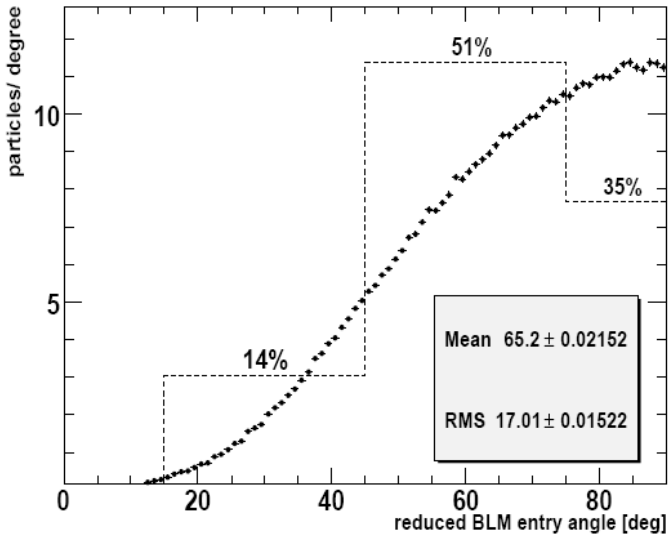

Fig.6.4.2: Angular binning; the dashed lines show the percentage contributions of the fluence convoluted with the four response functions [4].

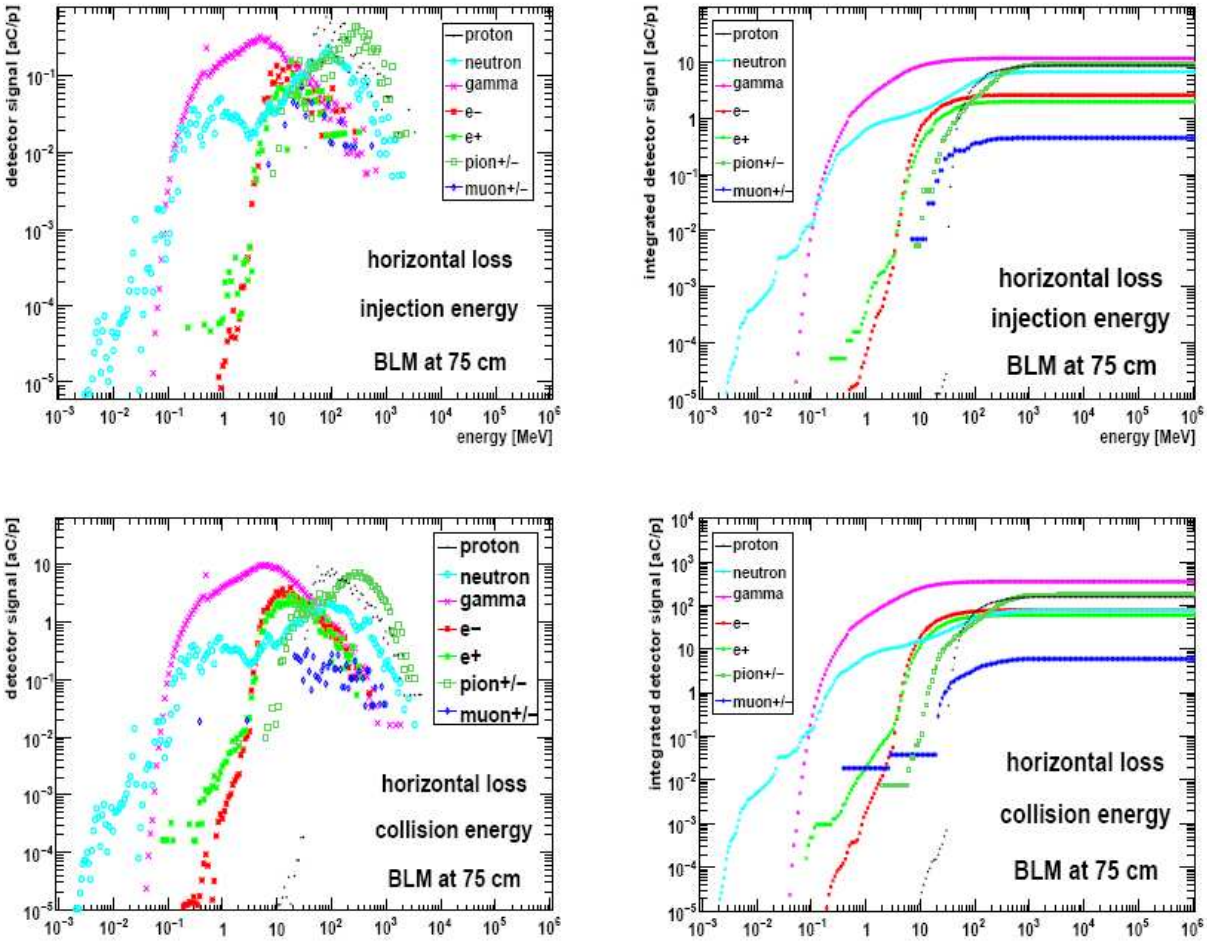

Fig.6.4.3: The signal in the BLM (per impacting proton) as a function of particle type and kinetic energy. 60 degree response function has been applied. On the left plots: raw signals are presented, on the right ones - integrated [4].

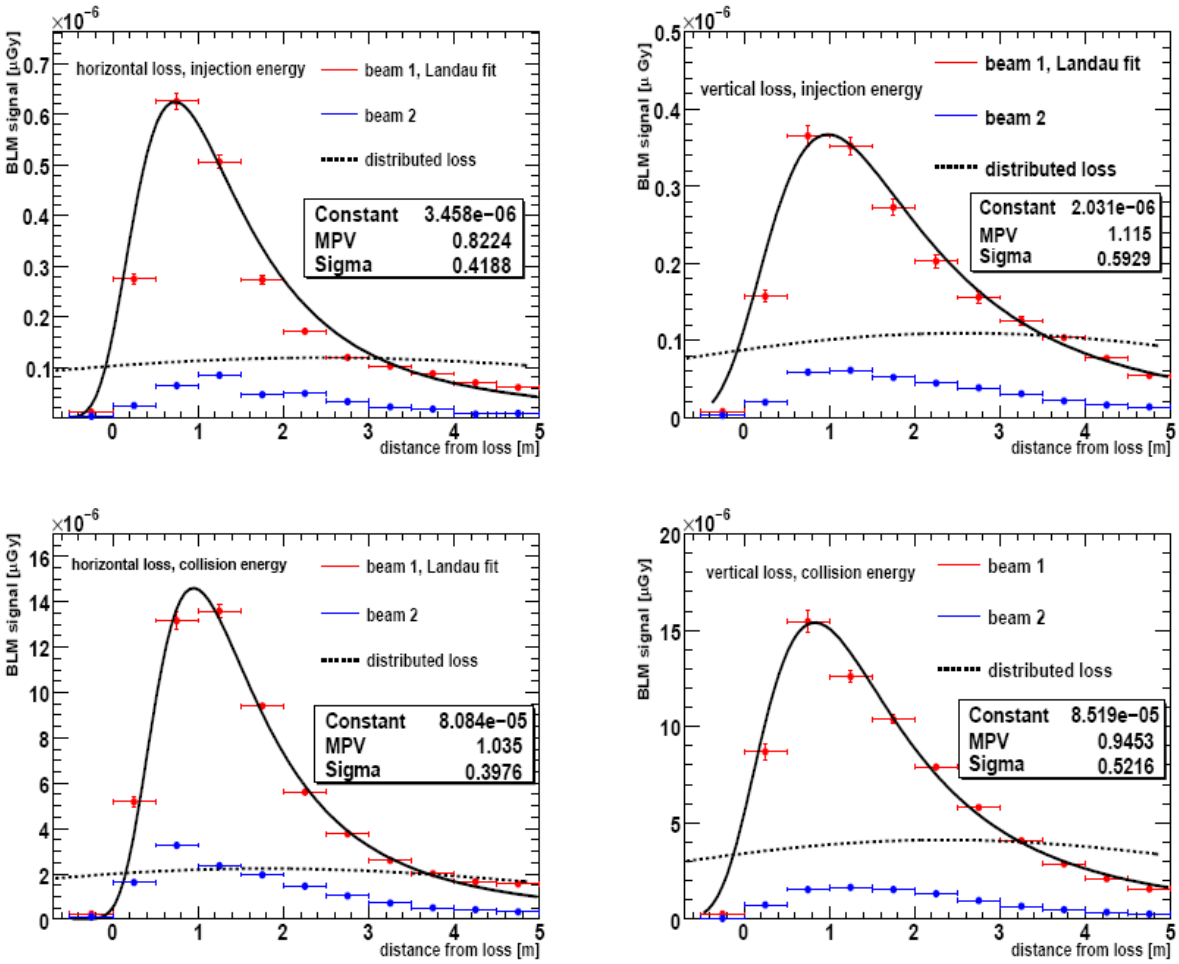

Fig.6.4.4: Beam Loss Monitor signals (per proton). Results shown for long tubes along the magnet. Red points corresponds to BLM registered particles from beam1 while blue points to opposite BLM. The dashed line points the signal in case of distributed losses [4].

At the end, the signal which would be measured by the beam loss monitors along the magnet is presented on Fig.6.4.4. The unit of the signal is Gray because detectors register absorbed radiation dose due to ionizing radiation. Landau distribution has been used owing to simulations of pointlike losses. The peak of the signal appears about 1 meter from the loss location and the full width at half maximum (FWHM) is roughly equal 2.5 meters. The signal FWHM is 4-5 times greater than in case of energy density distribution inside the coil.

Therefore, higher thresholds must be set for distributed losses than for concentrated ones.

Fig.6.4.5 gives a total view of particle contributions into the detector signal as a function of the distance from the loss location. In 1 meter from the energy release the most significant agents are photons, pions and protons. The impact of electrons, positrons and muons do not change considerably along the magnet. Moreover the contribution of muons

is almost neglectful. Neutrons play an important role at the beginning of the particle shower, especially in the case of the injection energy.

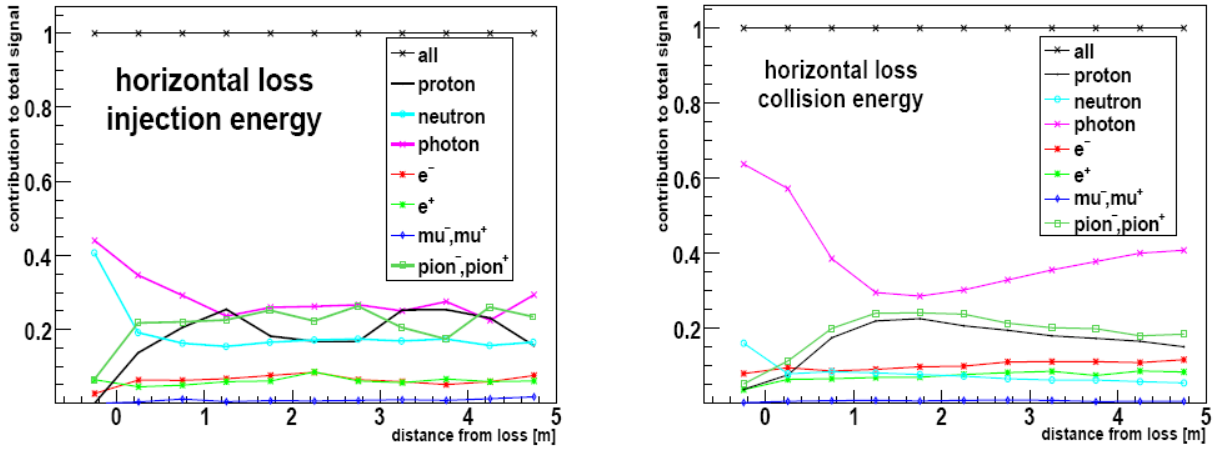

Fig.6.4.5: Secondary particles give different contribution to the total signal. Here the contribution of various particles to the normalized signal in detector is presented [4].

6.5 Quench prevention

Quench prevention is based on an accurate estimation of thresholds in the LHC data bases which would trigger the chain of protecting actions in case of emergency. These thresholds depend strongly on four parameters:

1) beam energy
2) type of loss (distributed or pointlike)
3) loss duration
4) loss location (with respect to detectors)

In this study only steady-state and fast transient losses have been considered. It must be mentioned that the locations of BLMs are not the same for every magnets – these are related to a magnet type and a magnet position in the arc.

Correlation between the energy deposition (E_D^{max}) in coils and the BLM signal outside the cryostat as a function of distance from loss location is shown on Fig.6.5.1. Summing up, the maximum of the energy density appears 35 cm from the loss location while BLM signal peaks about 65 cm further.

A quench-protecting threshold is denoted by *D* and given in Grays. It is directly measured by the Beam Loss Monitors and corresponds to the energy deposition in the superconducting coils.

As it is reported in [18], the quench-protecting thresholds can be calculated with the following equation:

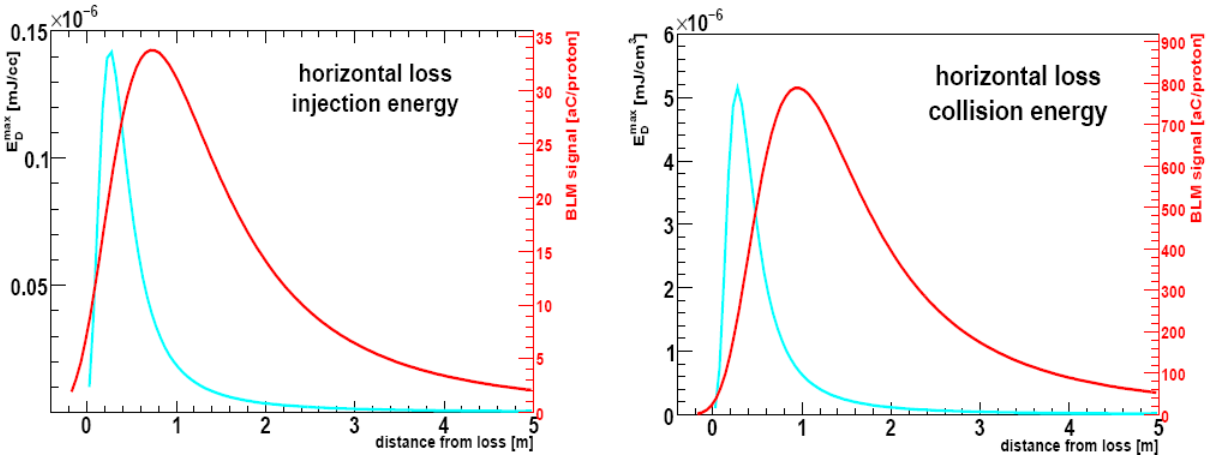

Fig.6.5.1: Correlation between the energy deposition in the coils and signal in BLMs [4].

$$D[Gy] = \left(C_{Gy}^{C}\right)^{-1}\left[Q_{BLM}\cdot H_{cable}\cdot\frac{1}{E_D^{max}}\right], \tag{6.5}$$

where $\left(C_{Gy}^{C}\right)$ is a conversion factor from Grays to the charge deposited in the BLM and is equal $5.4\cdot 10^{-4}\,{}^{C}/_{Gy}$, $Q_{BLM}$is the BLM signal, H_{cable} is a cable enthalpy. The most conservative values (studies in [4]) of the cable enthalpy have been chosen in calculations.

Table 6.5.1 contains threshold values as a dependence of distance between BLM and the loss location.

The BLM signal is greater is case of the collision energy than in case of the injection energy even by a factor of 42 and can be interpreted as an impact of strong magnetic field on the particle shower shape.

*Table 6.5.1: Signals in BLMs corresponding to single lost proton (*QBLM*) and to quench level for fast losses (*D*)[4].*

	horizontal loss				vertical loss			
	beam 1 right		beam 1 left		beam 1		beam 2	
BLM	inj	coll	inj	coll	inj	coll	inj	coll
at 25 cm								
Q_{BLM}[aC/prot]	10.9	279.3	8.8	67.7	8.5	469.4	1.1	39.9
D[μGy]	46.4	1.0	37.5	0.2	146.2	32.3	18.9	2.7
at 75 cm								
Q_{BLM}[aC/prot]	21.6	711.2	22.0	210.0	19.7	833.8	3.2	83.1
D[μGy]	92.0	2.4	93.7	0.7	338.9	57.5	55.1	5.7
at 125 cm								
Q_{BLM}[aC/prot]	22.8	734.0	21.9	212.6	19.0	679.9	3.3	89.2
D[μGy]	97.1	2.5	93.2	0.7	326.9	46.8	56.8	6.1
at 175 cm								
Q_{BLM}[aC/prot]	18.8	507.7	14.7	155.7	14.7	559.8	2.8	82.5
D[μGy]	80.1	1.7	62.6	0.5	252.9	38.6	48.2	5.7
at 225 cm								
Q_{BLM}[aC/prot]	11.8	302.7	9.2	110.4	10.9	425.9	2.4	71.3
D[μGy]	50.3	1.0	39.2	0.4	187.5	29.3	41.3	4.9
at 475 cm								
Q_{BLM}[aC/prot]	3.7	83.9	3.6	35.4	2.9	85.0	0.7	14.7
D[μGy]	15.8	0.9	15.1	0.1	49.9	5.9	12.0	1.0
Distributed losses								
Q_{BLM}[aC/prot]	6.2	145.5	5.0	50.8	5.1	190.3	1.0	24.6
D[μGy]	492	19.8	395	6.9	1394	154	266	19.9

7. Accuracy of the simulations

As this entire report indicates, the procedure of the high energy and accelerator physics the simulations is very sophisticated and consists of many steps at different scientific levels. This follows the possible sources of errors. The main ones are related to:

- E_D (10÷20%)
- Q_{BLM} (20% from the tail simulations and 5% from Monte Carlo statistics)
- H_{cable} (20%)
- statistics (about 5%)
- response functions (about 20%)

The independence of E_D^{max} and Q_{BLM} has been assumed. The uncertainty of signal coming from a single proton has been found as the most important factor. The Table 7.1 contains the summary of dominant uncertainties. The total error has been estimated of about 40%.

Table 7.1: Percentage contribution of different error sources [4].

E_{beam}	contribution from ΔQ_{BLM}	contribution from ΔH_{cable}	contribution from ΔE_D	total error
450 GeV	29%	20%	11%	37%
7 TeV	29%	20%	21%	41%

8. Conclusions

The development of the particle cascade caused by beam losses in the Main Dipole has been simulated with the Geant4 Monte Carlo Code. The main aim of this study has been to estimate the correlation between the energy deposition inside the superconducting coils and the signal in the Beam Loss Monitors. Various scenarios have been considered as regards to three main agents:

1) the beam energy (from 250 GeV up to 8 TeV),
2) the loss location (horizontal left, horizontal right, vertical upward)
3) the distance of detectors from the loss appearance.

The thresholds for fast losses have been estimated and the error sources has been discussed.

Detail investigations on the two first beam-induced quenches at LHC (made in [4]), which have been observed on 9^h of August and 7^{th} of September 2008 during the injection tests, have indicated that:

- the Gaussian fitting is a proper approximation if the cascade tail is negligible; this coincides with the situation when the cascade length is narrower than the Gaussian loss,
- the loss of the beam with $\sigma \approx 1$mm with the impact angle of 750 μrad produces the signal in the BLMs which has a long tail; for an angle of 250 μrad, the tail is mashed by the Gaussian shape of the loss,
- the simulations underestimates the BLM signal about 2-3 times (based on both quenches) for transient losses consisting of $4 \cdot 10^9$ protons,
- for small (~10^2 μrad) impacting angles the data should be fitted with the Landau curve,

Despite the fact that the estimated in Geant4 the BLM signals are 2.7-3.5 times smaller than ones measured, the thresholds protect magnets properly because the enthalpy limit of the cables caused to be 40-50% smaller than one calculated.

Steady-state losses have not been verified due to a lack of appropriate machine conditions.

These studies give a crucial information concerning the protection of the magnets - BLM setting thresholds have been already stored in LHC Software Architecture (LSA) database .

All of the above induces that further investigations need to be performed to set safe thresholds also on the other magnets.

The Geant4 geometries of the Main Quadrupole (MQ), the Wide aperture quadrupole (MQY) and the interconnections between MB and the Short Straight Section have been already implemented and the data analysis is foreseen soon.

Bibliography

[1] *LHC Design Report*, http://ab-div.web.cern.ch

[2] CERN Drawing Directory Server, http://lhc.web.cern.ch/lhc/

[3] The CERN Engineering & Equipment Management Service, http://lhc.web.cern.ch/lhc/

[4] B. Dehning, A. Priebe, M. Sapinski, *Simulation of Beam Loss in LHC MB Magnet and Quench threshold test, CERN-LHC-Project-Note-422*, CERN, Geneve 2009

[5] S. Russenschuck, *1st International Roxie Users Meeting and Workshop - ROXIE: routine for the optimization of magnet X-sections, inverse field calculation and coil end design*, CERN yellow report 99-01, CERN, Geneve, 1999

[6] D. Bocian, EDMS no 750204, CERN, Geneve, 2006

[7] A. Stockner, PhD thesis, CERN, Geneve, 2007

[8] S.Y.Lee „*Accelerator Physics*" (Second Edition), World Scientific, Singapore, 2004

[9] A.W.Chao, M.Tigner "*Handbook of Accelerator Physics and Engineering*", World Scientific, Singapore, 2006

[10] R.Denz "*Quench Protection System*"

[11] K.H.Mess "*Quench Protection*" , CERN Summer Student Lectures, Geneve

[12] P. Schmüser "*Superconductivity*", Summer Student Lectures, Geneve

[13] *LHC the guide – CERN faq*, CERN, Geneve, 2008

[14] J.B. Jeanneret, D. Leroy, L. Oberli, T. Trenkler, "*Quench levels and transient beam losses in LHC magnets*". LHC Project Report 44, CERN, Geneve

[15] www.cm.ph.bham.ac.uk

[16] http://lhc.web.cern.ch/lhc/

[17] Nikolai Schwerg, private communication, CERN, Geneve

[18] B. Dehning, private communication, CERN, Geneve

[19] Valerii M. Vinokur, Tatyana I. Baturina, Mikhail V. Fistul, Aleksey Yu. Mironov, Mikhail R. Baklanov & Christoph Strunk "*Superinsulator and quantum synchronization*"; Nature 452, 613-615

[20] D.H.Perkins *"Wstęp do fizyki wysokich energii"*, PWN, Warszawa 2004

Abbreviations

BLM - Beam Loss Monitoring System

CDD - CERN Drawing Directory Server

CERN - The European Organization for Nuclear Research *(*originally*: Conseil Européen pour la Recherche Nucléaire)*

DS - Dispersion Suppressor

EDMS - CERN Engineering & Equipment Management Service

HEP - High Energy Physics

LEP - The Large Electron-Positron collder

LHC - The Large Hadron Collider

LSS - Long Straight Section

LINAC - Linear Particle Accelerator

MB - Main Dipole

MQ - Main Quadrupole

QPS - Quench Prevention System

PS - Proton Synchrotron

RF - Radio Frequency

SC - Superconductor

SEM - Secondary Emission Monitos

SSS - Short Straight Section

SPS - Super Proton Synchrotron

Index of Figures

Index of Tables

Appendix A

Example of a calculating the weighted density of complex materials. The case of an outer layer MB coils.

Known:

- ➔ Copper to superconductor (SC) ratio: 1.95
- ➔ Nb: 53% ; density: 8.57 g/cm^3
- ➔ Ti: 47% ; density: 4.51 g/cm^3
- ➔ Cu density 8.96 g/cm^3
- ➔ liquid He: 5% (between cables) ; density: 0.125 g/cm^3 (thus 95% of the entire mass is represented by Cu-NbTi component)

Thus Nb-Ti density:

$$d = \frac{d_{Nb} \cdot 53\% + d_{Ti} \cdot 47\%}{100\%} = 6.6618 \ {}^{g}/_{cm^3}$$

Then Cu-NbTi density:

$$\frac{m_{Cu}}{m_{Nb-Ti}} = \frac{1.95}{1} \rightarrow m_{Cu} = 1.95 \, m_{Nb-Ti}$$

$$m_{Cu} + m_{SNb-Ti} = 100\%$$

Percentage amount of superconductor have been obtained from proportion:

$$2.95 \rightarrow 100\%$$

$$1.95 \rightarrow x\%$$

$$x = 66.10\% \, Cu$$

$$d_{Cu-NbTi} = \frac{66.10\% \cdot d_{Cu} + 33.90\% \cdot d_{Nb-Ti}}{100\%} = 8.18 \, {}^{g}/_{cm^3}$$

Subsequently He-Cu-NbTi density:

$$d_{Cu-NbTi} = \frac{5\% \cdot d_{liquidHe} + 95\% \cdot d_{Cu-NbTi}}{100\%} = 7.78 \, {}^{g}/_{cm^3}$$

.

Also a percentage composition of material is a significant element for Geant4 simulations and has been calculated from proportion as follows:

$$Cu - NbTi \rightarrow 100\%$$

$$100\%\ Cu - NbTi \rightarrow 66.10\%\ Cu$$

$$95\%\ Cu - NbTi \rightarrow x$$

$$x = 62.80\%\ Cu$$

$$100\%\ Cu - NbTi \rightarrow 33.90\%\ Cu$$

$$95\% \rightarrow y$$

$$y = 32.20\%\ NbTi$$

$$100\% NbTi \rightarrow 47\% Ti$$

$$100\%\ NbTi \rightarrow 47\%\ Ti$$

$$32.20\% \rightarrow\ z_1$$

$$z_1 = 15.13\ Ti$$

$$100\%\ NbTi \rightarrow 53\%\ Nb$$

$$32.20 \rightarrow z_2$$

$$z_2 = 17.07\%\ Nb$$

It's obvious that in total all factors must give 100% - otherwise during a compilation system returns error (a tip for errors which are difficult to specify ;))

All complex materials (different SC coil materials, epoxy impregnated fiberglass etc) have been calculated with the same procedure.

Selected CDD Drawings

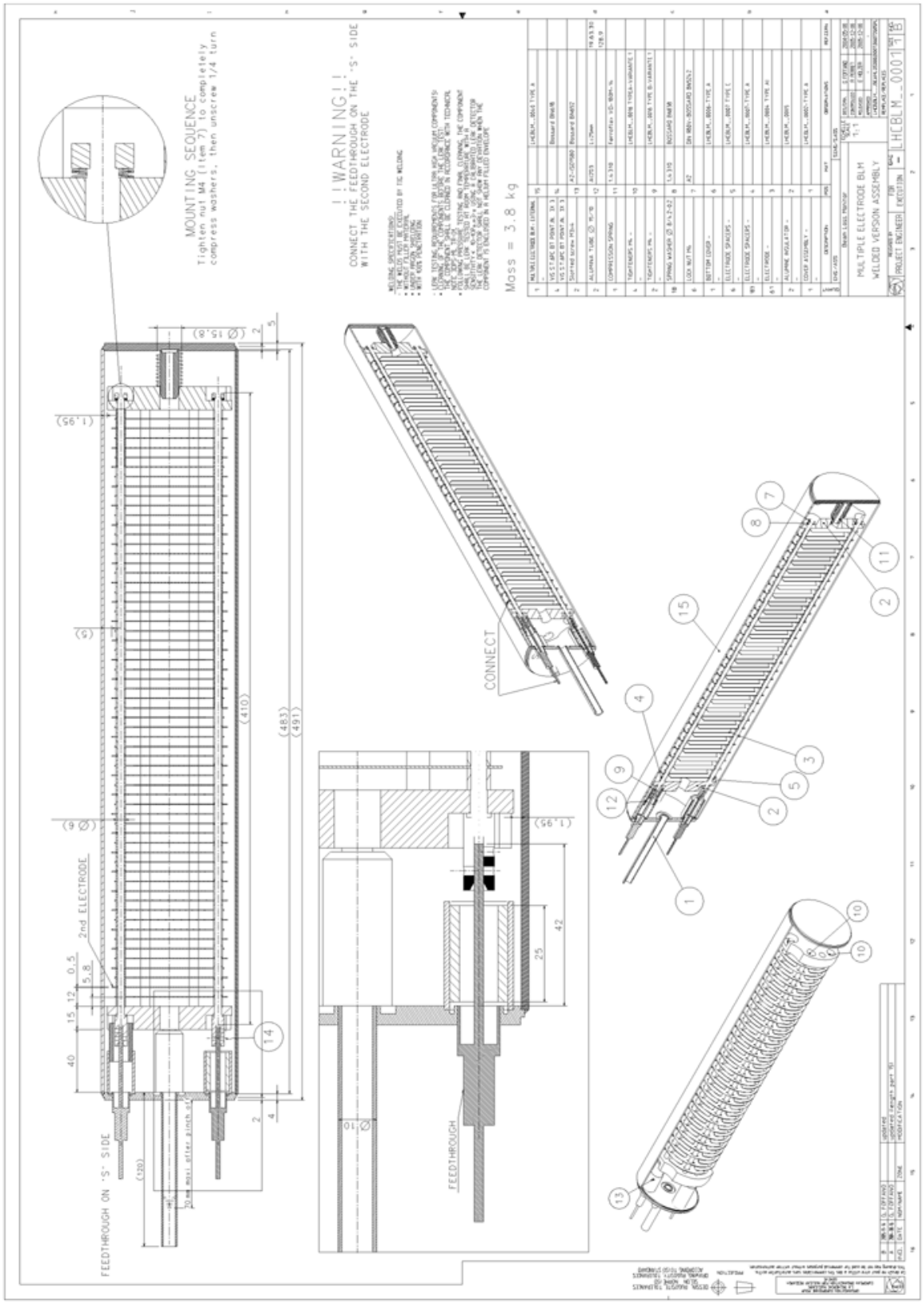

LHCBLM__0001

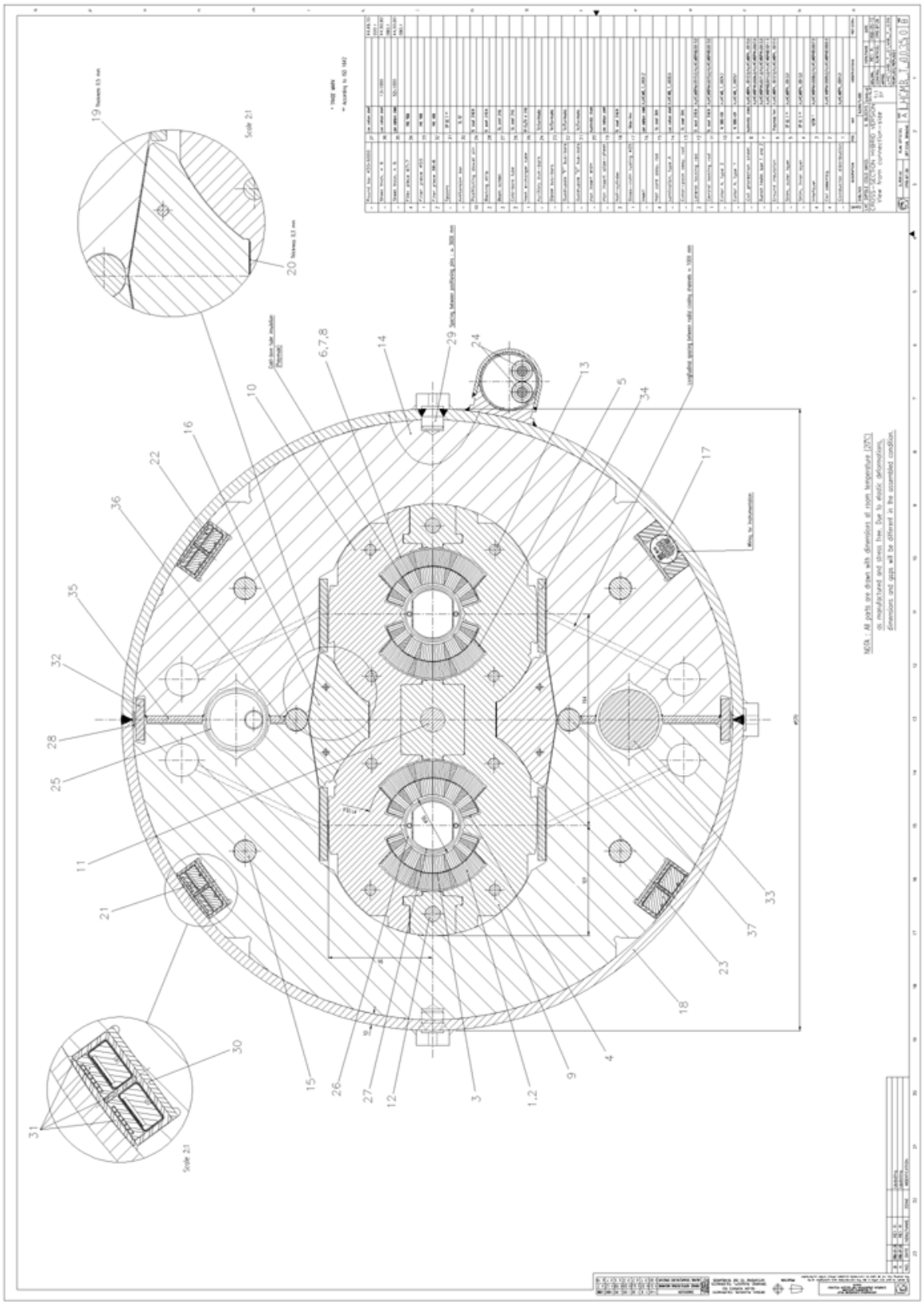

LHCMB_T_0035

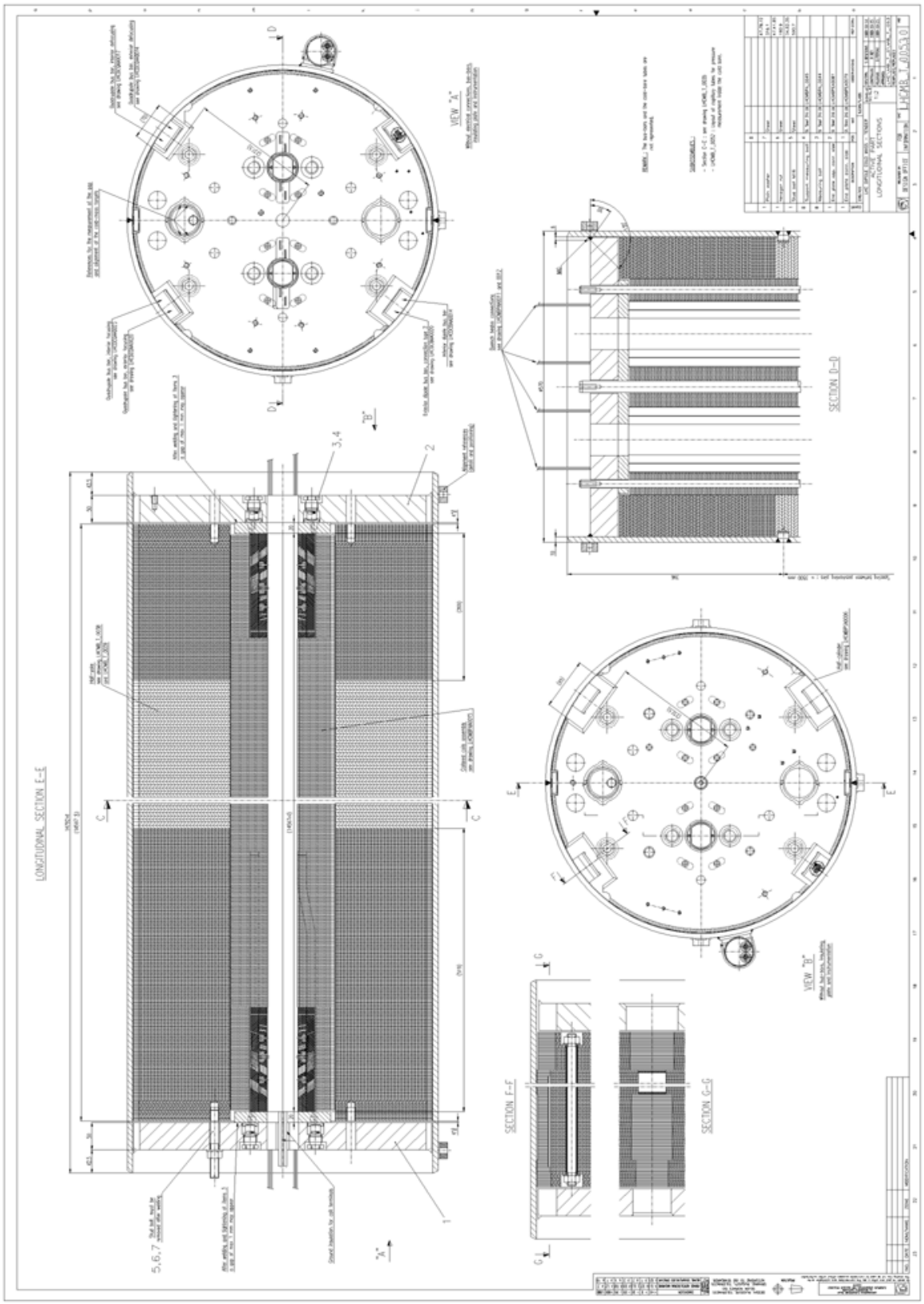

LHCMB_T_053

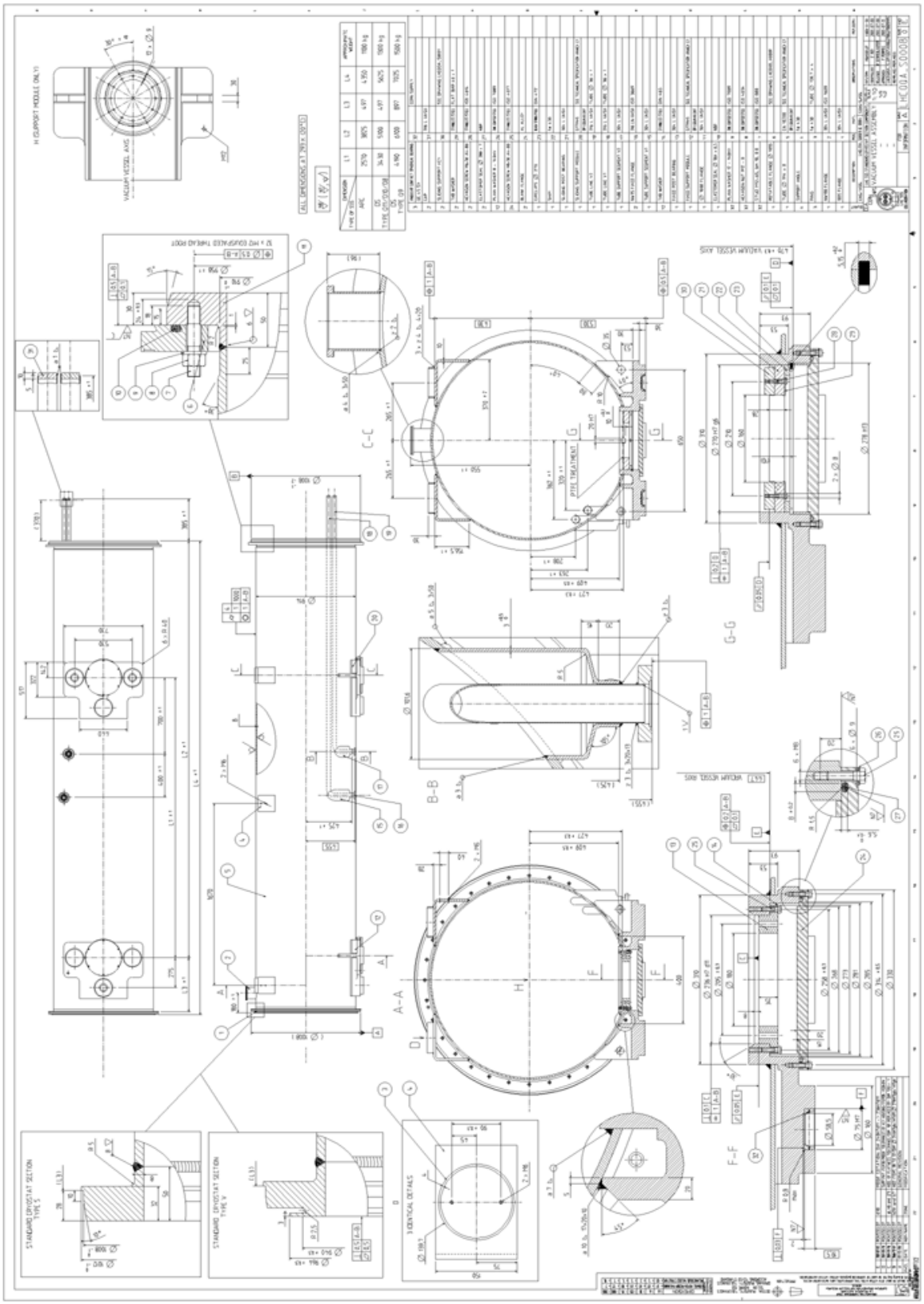

LHCQQA_S0008

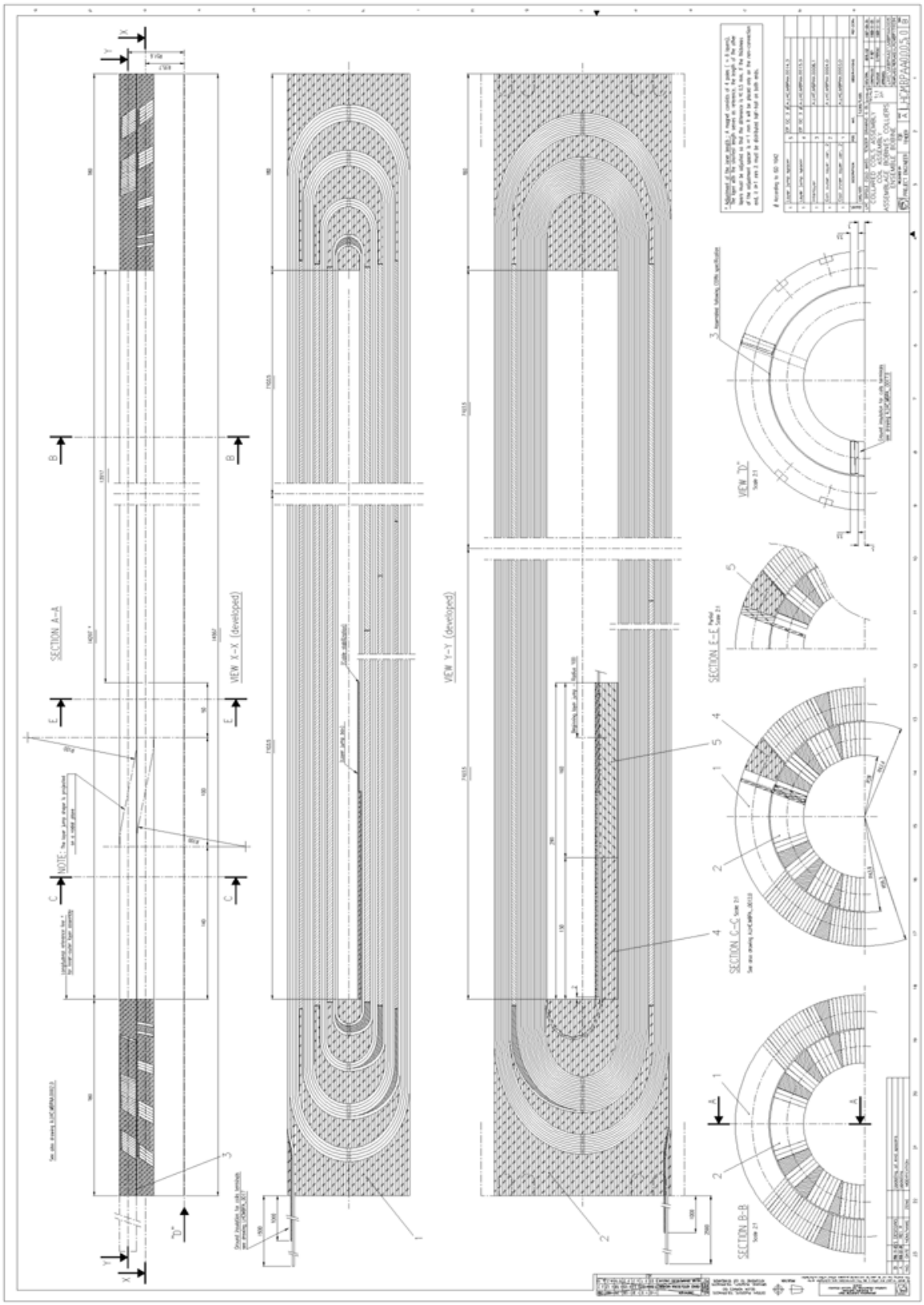

LHCMBPAA0005